

Article 05

Article 5 :

Publié dans la revue *Journal of Vibration Engineering & Technologies*

- **Éditeur :** Springer Nature
- **ISSN :** 2523-3920 **E-ISSN :** 2523-3939
- **Domaine scientifique :** Génie civile et mécanique
- **Type de source :** Revue classée A (*lien :* https://www.dgrsdt.dz/fr/revues_A?search=2523-3939#search_engine)



وزارة التعليم العالي والبحث العلمي



الجمهورية

Français



The screenshot shows the official website of the Researcher Scientific Development and Transfer (RSDT). The header features the logo of the Ministry of Higher Education and Scientific Research, the RSDT logo, and links for French, social media, and calls. Below the header, a banner highlights 'Revues scientifiques de catégorie A'. The main content area displays a grid of journal covers, with one specific journal, 'JOURNAL OF VIBRATION ENGINEERING & TECHNOLOGIES', highlighted with a red border.

JOURNAL OF VIBRATION ENGINEERING & TECHNOLOGIES

Résultat :1

Télécharger

TITRE DE LA REVUE--

EDITEUR

ISSN

EISSN

JOURNAL OF VIBRATION
ENGINEERING & TECHNOLOGIES

SPRINGER HEIDELBERG

2523-3920

2523-3939



A new trigonometric shear deformation theory for static and free vibration responses of laminated plates using strain-based approach.

Taqiyeddine Assas ^{1,*} · Messaoud Bourezane ¹ · Madjda Chenafi ¹ · Seyfeddine Benabid ²

Received: 03 July 2025 / Revised: 29 September 2025 / Accepted: 07 November 2025
© The Author(s) 2025

Abstract

The primary objective and novelty of this paper is to develop a new quadrilateral four-node finite element based on the strain-based Trigonometric Shear Deformation Plate Theory (TrSDPT) for the static and free vibration analysis of laminated composite plates. This is the first element based on a strain-based high-order shear deformation theory (HSDT) for analyzing static and free vibration behaviors of laminated plates. The main innovation lies in reducing the unknowns to five degrees of freedom per node by enforcing zero transverse shear stresses on the top and bottom surfaces and assuming a sinusoidal shear strain distribution, thus avoiding any shear correction factor. The developed element effectively combines membrane and bending strain formulations to enhance accuracy and efficiency. Numerical studies on symmetric and antisymmetric laminated plates with different geometries and boundary conditions show displacement errors below 2% and natural frequency deviations within 1.5%, confirming the proposed element's excellent precision, stability, and computational performance.

Keywords Static. Free vibration. Trigonometric shear deformation. Composite plates. Strain-based

Taqiyeddine Assas, Messaoud Bourezane, Madjda Chenafi and Seyfeddine Benabid contributed equally to this work.

✉ Taqiyeddine Assas
taqiyeddine.assas@univ-biskra.dz
Messaoud Bourezane
mess.bourezane@univ-biskra.dz
Madjda Chenafi
madjda.chenafi@univ-biskra.dz
Seyfeddine Benabid
seyfedine.benabid@univ-biskra.dz

¹ Laboratoire d'Aménagements Hydrauliques et Environnement (LAHE), Département de Génie Civil et Hydraulique, Université de Biskra, B.P. 145, R.P. 07000 Biskra, Algeria

² Research Laboratory in Subterranean and Surface Hydraulic, LARHYSS, University of Biskra, Algeria.

Introduction

Laminated composite materials are increasingly being used in a wide range of engineering applications including aerospace, automobiles, civil engineering and biomedical due to their superior properties such as high strength, low weight and extended fatigue life. These materials have garnered significant attention due to their ability to meet the demanding performance criteria in these sectors[1].

Numerous analytical models have been developed to gain a deeper understanding of the mechanical response of laminated composites subjected to various loading conditions. These models can generally be divided into two main categories: three-dimensional (3D) elasticity models [2,3], which provide detailed and accurate representations of composite behavior but are often computationally intensive; and two-dimensional (2D) models, which include approaches such as the Equivalent Single-Layer (ESL) [4], layer-wise [5,6], zigzag [7,8], and quasi-three-dimensional approaches [9,10]. While 3D models provide high-fidelity results, their application to real-world

problems is often limited because of the complexity of the geometry, the arbitrary boundary conditions, and the large calculation effort. As a result, a number of ESL-based plate models are proposed and commonly used in analytical mechanics to analyze the structural response of composite plate systems. Among these, the classic layered plate theory (CLPT), which relies on the Kirchhoff-Love hypotheses stands out as a simple yet effective method for analyzing thin laminated plates. It does not account for transverse shear effects, which limits its accuracy in thicker plates. To address this limitation, the First-Order Shear Deformation Theory (FSDT) was developed, which incorporates transverse shear effects and is applicable to both thin and moderately thick plates. FSDT requires the introduction of a shear correction factor (SCF), which can be challenging to calculate and is influenced by factors such as loadings, geometry, material properties, and boundary conditions. As a result, many HSDTs were proposed to address the limited capabilities of CLPT and FSDT. These include the third (TSDT)[11-14], trigonometric (TrSDT)[15-18], exponential (ESDT)[19, 20, 21], and hyperbolic shear deformation theory (HSDT) [22-25], plate theories (RPT) [26,27]. In recent years, considerable advancements in computational modeling in structural and energy systems engineering have been dedicated to the development of robust and precise numerical models aimed at analyzing complex behaviors under varying operational conditions. For example, Suleyman Adak [28] investigated the power factor variation of grid-connected photovoltaic systems under different irradiance levels throughout the day using MATLAB/Simulink modeling, demonstrating the effectiveness of numerical approaches in predicting dynamic system responses.

In addition to advances in energy systems modeling, significant progress has also been achieved in the vibration analysis of structural and plate systems. Recent studies have focused on developing efficient numerical and analytical models to capture complex vibration behavior under arbitrary boundary and loading conditions. For instance, Zhou *et al.* [29] developed a spectral element model for the free vibration of orthotropic rectangular Mindlin plates with arbitrary boundaries. Tran *et al.* [30] proposed a new thermoelastic model for temperature-dependent vibration analysis of functionally graded CNT-reinforced plates. Similarly, Zhou *et al.* [31] investigated the bandgap characteristics of periodic Mindlin plates via the Spectral Element Method, while Qin *et al.* [32] applied advanced optimization algorithms to vibration-based condition assessment of steel-concrete composite bridges. Moreover, Qin *et al.* [33] proposed a refined Hilbert-transform-based approach for modal parameter identification in civil structures. These recent contributions emphasize the growing research interest in vibration modeling and analysis of structural systems, reinforcing the relevance of developing robust and computationally efficient finite element formulations such as the one proposed in this study.

Similarly, in the field of structural mechanics, several numerical techniques have been developed to analyze the behavior of composite plates, such as the Finite-Element Method (FEM)[34,35,36], Isogeometric Analysis (IGA)[37-40], mesh-free methods[41,42,43], Boundary Element Method (BEM)[44,45,46], and the Smoothed Finite Element Method (S-FEM) [47-51]. Among these, FEM has gained recognition as a reliable and effective computational tool for the investigation of composite laminates plates, as demonstrated by the works of Katili et al.[52]. In particular, FEM based on the strain approach has gained significant importance in the domain of computational solid state mechanics. In this approach, the displacement field of finite elements is defined by an assumed function for the various

components of the strain field, ensuring the satisfaction of compatibility equations. The strain-based approach offers several advantages, such as the direct fulfillment of the two primary convergence criteria related to strains (constant strains and rigid body motion). Additionally, it allows for enriching the displacement field with higher-order terms without the need for adding intermediate nodes or unnecessary degrees of freedom. This method is particularly effective in addressing issues like parasitic errors, mesh distortion, and various locking phenomena [53]. As an alternative to displacement-based models, finite elements based on the strain approach emerged in the early 1970s. The first elements developed were focused on curved elements[54,55]. This approach was later extended to plane elasticity elements[56,57,58], three-dimensional elasticity[59,60,61], and plate bending [62-63]. This development offered a more directe and efficient way to model deformation behavior in various structural problems. It is worth emphasizing that all previously developed plate elements based on the strain approach were limited to isotropic materials using the First-Order Shear Deformation Theory (FSDT). In contrast, the present study introduces, for the first time, a novel strain-based finite element formulated within the context of a Higher-Order Shear Deformation Theory (HSDT) for the analysis of laminated composite plates, thereby addressing this research gap.

This study presents a four-node quadrilateral element formulated using a strain-based ESL model within the framework of TrSDPT. It is specifically designed to investigate the bending and dynamic behavior of laminated plates with square, skewed, and elliptical geometries. Unlike standard HSDT approaches that use more than five variables, this method simplifies the model to just five unknowns by assuming a sinusoidal shear strain distribution and setting the transverse shear stress to zero on the top and bottom surfaces. The newly developed element, named HSBQLP20 (High-Order Strain-Based Quadrangular Laminated Plate element featuring 20 unknowns), has five primary Dofs ($u, v, w, \beta_x, \beta_y$) in its four node corners. The displacements shape fileds of the component is constructed using a polynomial function with 20 coefficients, accurately representing both rigid body and deformation modes, while ensuring compatibility with the element's strain equations. The impact of several plate parameters including the number of layers, aspect ratio, fiber orientation, and boundary conditions has been investigated. The results, represented in terms of transverse displacements and natural frequencies, are evaluated across different parameter sets. In order to validate the accuracy of the current study, the obtained findings have been compared with existing data from the published literature. Figure 1 presents a block diagram summarizing the overall structure of the paper, highlighting the problem definition and motivation, theoretical development, finite element formulation, validation through numerical results, and concluding remarks.

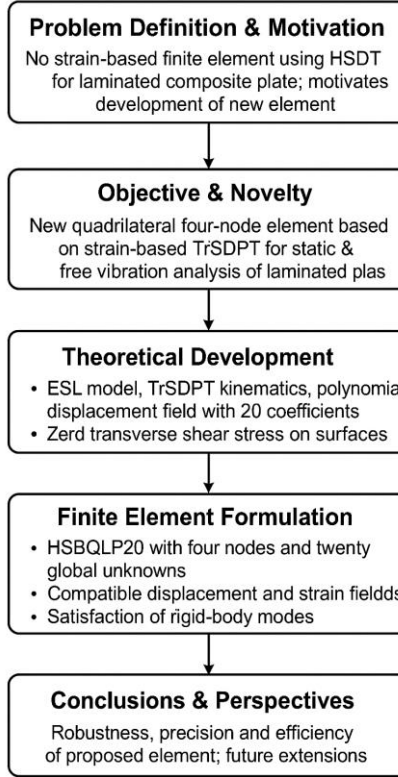


Figure 1. Block diagram summarizing the methodology of the present study.

1. Theoretical formulations

1.1 Displacements and strains

The displacement fields (u, v, w) in the x, y, and z directions for moderately thick plates can be described as follows [64,65] :

$$\begin{aligned} u(x, y, z) &= u_0(x, y) + z\beta_x(x, y) \\ v(x, y, z) &= v_0(x, y) + z\beta_y(x, y) \\ w(x, y, z) &= f(z)w_0(x, y) + (f(z)-1)R(x, y) \end{aligned} \quad (1)$$

$$\text{With } \beta_x(x, y) = \frac{\partial R(x, y)}{\partial x}; \beta_y(x, y) = \frac{\partial R(x, y)}{\partial y} \text{ and } f(z) = \frac{2\sqrt{5}}{3} \left(1 - \cos^2 \left(\frac{2\pi z}{h} \right) \right)$$

Where, u_0 and v_0 represent the central displacements of the plate in the x- and y-axis, respectively. w_0 is the transverse displacement component. The rotational directions around the x- and y-axis are denoted by β_y and β_x , respectively. The function $f(z)$ describes the shape functions that determine how transverse shear strains and stresses vary through the plate's thickness. This function provides that the lateral shear stresses are null at the upper as well as at the lower surface of the plate.

In the literature, numerous types of shape functions have been proposed, including polynomial, trigonometric, exponential, and hyperbolic forms. Representative examples of these functions are presented in Table 1.

Table 1. Shear deformation shape functions.

Auteur / Modèle	Fonction $f(z)$	Type de fonction	Condition
			$\tau_{xz} = \tau_{yz} = 0$
			$a z = \pm \frac{h}{2}$
Reddy [12]	$f(z) = z - \frac{4z^3}{3h^2}$	Polynômiale cubique	✓
Hosseini-Hashemi [66]	$f(z) = z e^{(-2(\frac{z}{h})^2)}$	Exponentiel	✓
Dorgan et al [67]	$f(z) = z(\cosh(\frac{z}{h}) - 1.388)$	Hyperbolique	✓
Soldatos[68]	$f(z) = h \sinh(z/h) - z \cosh(1/2)$	Hyperbolique	✓
Mechab et al. [69]	$f(z) = \frac{z \cos(1/2)}{-1 + \cos(1/2)} - \frac{h \sin(z/h)}{-1 + \cos(1/2)}$	Trigonométrique	✓
Présent travail (TrSDPT)	$f(z) = \frac{2\sqrt{5}}{3} \left(1 - \cos^2 \left(\frac{2\pi z}{h} \right) \right)$	Trigonométrique	✓

The introduced shape function is an odd function with respect to the thickness coordinate z , and it satisfies the zero transverse shear stress conditions at the upper and lower surfaces of the plate. As shown in Table 1, the proposed function belongs to the class of simple analytical expressions, which greatly simplifies the integration process and, consequently, reduces the computational time. Since the function is analytically integrable, there is no need for numerical integration, thus enhancing the accuracy and stability of the obtained results.

The validity of these claims is demonstrated in Figure 2, where comparative diagrams of the newly introduced shape function and those listed in Table 1 are presented.

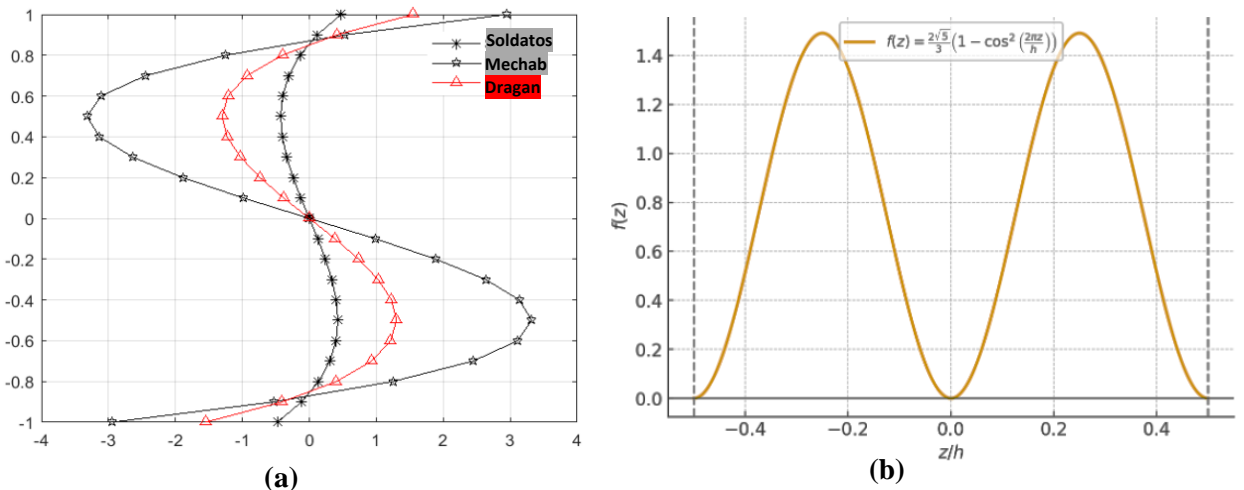


Figure 2. Shape function diagrams: (a) shape functions from the literature; (b) newly proposed shape function.

The expression for the in-plane strain vector $\{\varepsilon\}$ is given by :

$$\{\varepsilon\} = \begin{Bmatrix} \varepsilon_x \\ \varepsilon_y \\ \gamma_{xy} \end{Bmatrix} = \{\varepsilon^0\} + z\{\kappa\} \quad (2)$$

The lateral shear strain $\{\gamma\}$ is defined as :

$$\{\gamma\} = \begin{Bmatrix} \gamma_{xz} \\ \gamma_{yz} \end{Bmatrix} = f(z)\{\gamma^0\} \quad (3)$$

Where $\{\varepsilon^0\}$, $\{\kappa\}$ and $\{\gamma^0\}$ are membrane, bending strains and the transverse shear strain vectors, respectively.

$$\{\varepsilon^0\} = \begin{Bmatrix} \varepsilon_x^0 \\ \varepsilon_y^0 \\ \gamma_{xy}^0 \end{Bmatrix} = \begin{Bmatrix} \frac{\partial u}{\partial x} \\ \frac{\partial v}{\partial x} \\ \frac{\partial u}{\partial y} + \frac{\partial v}{\partial x} \end{Bmatrix}; \{\kappa\} = \begin{Bmatrix} \kappa_x \\ \kappa_y \\ \kappa_{xy} \end{Bmatrix} = \begin{Bmatrix} \frac{\partial \beta_x}{\partial x} \\ \frac{\partial \beta_y}{\partial y} \\ \frac{\partial \beta_x}{\partial y} + \frac{\partial \beta_y}{\partial x} \end{Bmatrix}; \{\gamma^0\} = \begin{Bmatrix} \gamma_{xz}^0 \\ \gamma_{yz}^0 \end{Bmatrix} = \begin{Bmatrix} \frac{\partial w}{\partial x} + \beta_x \\ \frac{\partial w}{\partial y} + \beta_y \end{Bmatrix} \quad (4)$$

2.2 Stress-strain relationships

In composite laminated plates, each layer is orthotropic and defined in a local (1, 2, 3) coordinate system. Directions 2 and 3 are considered isotropic within the plane (**Figure. 3a**), where 1 is the fiber direction, 2 is in-plane and perpendicular to the fibers, and 3 is the perpendicular to the plate. The assumption of plane stress ($\sigma_3 = 0$) is applied to all layers [34].

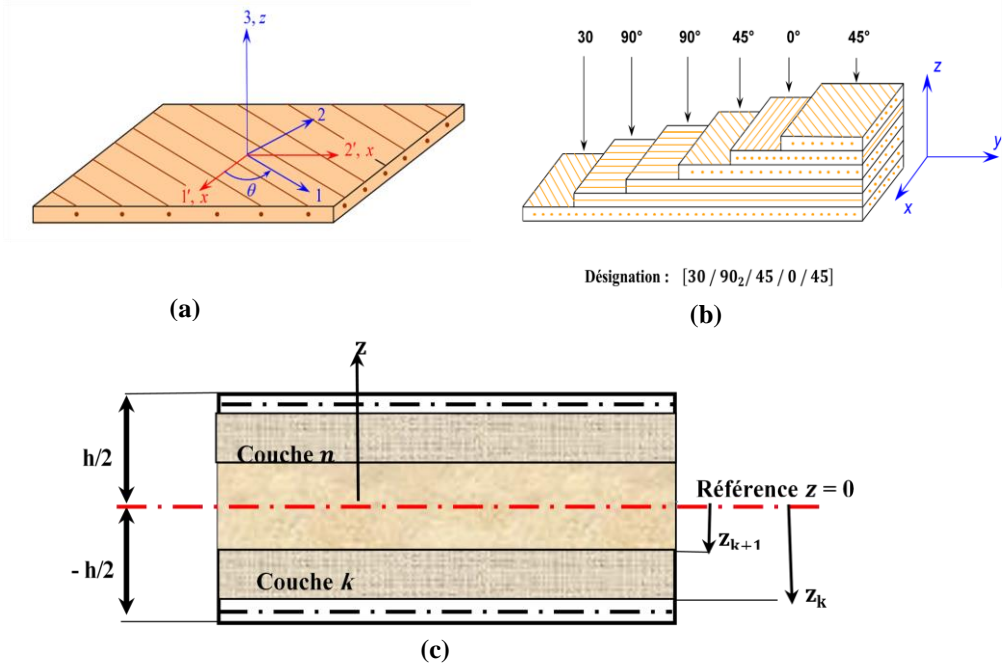


Figure 3. **a).** Orthotropic plate. **b).** The laminate plate designation. **c)** Layer arrangement and numbering for a typical laminated plate.

In the local coordinate system (1-2-3), the stress-strain behavior of a planar orthotropic material is described by the following constitutive relation[70]:

$$\{\sigma_1\} = [C_b]\{\varepsilon_1\}; \{\tau_1\} = [C_s]\{\gamma_1\} \quad (5)$$

Where

$$\{\sigma_1\} = \begin{Bmatrix} \sigma_{11} \\ \sigma_{22} \\ \sigma_{12} \end{Bmatrix} = \begin{Bmatrix} C_{11} & C_{12} & 0 \\ C_{21} & C_{22} & 0 \\ 0 & 0 & C_{66} \end{Bmatrix} \begin{Bmatrix} \varepsilon_{11} \\ \varepsilon_{22} \\ \gamma_{12} \end{Bmatrix}; \{\tau_1\} = \begin{Bmatrix} \tau_{13} \\ \tau_{23} \end{Bmatrix} = \begin{Bmatrix} C_{44} & 0 \\ 0 & C_{55} \end{Bmatrix} \begin{Bmatrix} \gamma_{13} \\ \gamma_{23} \end{Bmatrix} \quad (6)$$

And the elastic constants C_{ij} define the elastic behavior relative to the material's principal axes [34]:

$$C_{11} = \frac{E_1}{1 - \nu_{12}\nu_{21}}; C_{12} = \frac{\nu_{12}E_1}{1 - \nu_{12}\nu_{21}}; C_{22} = \frac{E_2}{1 - \nu_{12}\nu_{21}}; C_{66} = G_{12}; C_{55} = G_{23}; C_{44} = G_{13} \quad (7)$$

In Eq. (7), for each layer E_1 , E_2 and E_3 are the axial Young's moduli in the in-plane direction corresponding to the main material axes, while ν_{12} and ν_{21} are the major and minor Poisson's ratio in the plane, respectively. The shear moduli are defined as G_{12} for the in-plane direction, and G_{13} and G_{23} for the transverse directions. Considering that the laminated plate is composed of multiple orthotropic plies, each with the main material axes arbitrarily oriented with respect to the global laminate coordinate system (x , y , z), the constitutive relations for each ply must be transformed accordingly. Thus, the stress-strain relationships for the k -th off-axis layer (see Figure. 3c), expressed in the coordinate system of the laminate, are obtained by[70] :

$$\{\sigma\}^{(k)} = \begin{Bmatrix} \sigma_{xx} \\ \sigma_{yy} \\ \tau_{xy} \end{Bmatrix}^{(k)} = \begin{Bmatrix} \overline{C}_{11} & \overline{C}_{12} & \overline{C}_{16} \\ \overline{C}_{21} & \overline{C}_{22} & \overline{C}_{26} \\ \overline{C}_{61} & \overline{C}_{62} & \overline{C}_{66} \end{Bmatrix}^{(k)} \begin{Bmatrix} \varepsilon_{xx} \\ \varepsilon_{yy} \\ \varepsilon_{xy} \end{Bmatrix}^{(k)}; \{\tau\}^{(k)} = \begin{Bmatrix} \tau_{xz} \\ \tau_{yz} \end{Bmatrix}^{(k)} = \begin{Bmatrix} \overline{C}_{44} & \overline{C}_{45} \\ \overline{C}_{54} & \overline{C}_{55} \end{Bmatrix}^{(k)} \begin{Bmatrix} \gamma_{xz} \\ \gamma_{yz} \end{Bmatrix}^{(k)} \quad (8)$$

$$\{\sigma\}^{(k)} = [\overline{C}_b]^{(k)} \{\varepsilon\}^{(k)}; \{\tau\}^{(k)} = [\overline{C}_s]^{(k)} \{\gamma\}^{(k)} \quad (9)$$

Where $[\overline{C}_b]^{(k)}$ and $[\overline{C}_s]^{(k)}$ represent the transformed material constants for bending and shear of the k -th lamina, respectively.

$$[\overline{C}_b]^{(k)} = [T_b]^T [C_b][T_b]; [\overline{C}_s]^{(k)} = [T_s]^T [C_s][T_s] \quad (10)$$

While the transformation matrices $[T_b]$ and $[T_s]$ are given as :

$$[T_b] = \begin{bmatrix} \cos^2 \theta_k & \sin^2 \theta_k & \cos \theta_k \sin \theta_k \\ \sin^2 \theta_k & \cos^2 \theta_k & -\cos \theta_k \sin \theta_k \\ -2 \cos \theta_k \sin \theta_k & 2 \cos \theta_k \sin \theta_k & \cos^2 \theta_k - \sin^2 \theta_k \end{bmatrix}; [T_s] = \begin{bmatrix} \cos \theta_k & \sin \theta_k \\ -\sin \theta_k & \cos \theta_k \end{bmatrix} \quad (11)$$

2.3 The force and moment resultants

The forces and moments per unit length, represented as functions of the stress components across the thickness, obtained from[71]:

$$\begin{aligned}
\begin{Bmatrix} N_x \\ N_y \\ N_{xy} \end{Bmatrix} &= \int_{-\frac{h}{2}}^{\frac{h}{2}} \begin{Bmatrix} \sigma_x \\ \sigma_y \\ \tau_{xy} \end{Bmatrix} dz = \sum_{k=1}^n \int_{z_k}^{z_{k+1}} \begin{Bmatrix} \sigma_x \\ \sigma_y \\ \tau_{xy} \end{Bmatrix} dz; \\
\begin{Bmatrix} M_x \\ M_y \\ M_{xy} \end{Bmatrix} &= \int_{-\frac{h}{2}}^{\frac{h}{2}} \begin{Bmatrix} \sigma_x \\ \sigma_y \\ \tau_{xy} \end{Bmatrix}(z) dz = \sum_{k=1}^n \int_{z_k}^{z_{k+1}} \begin{Bmatrix} \sigma_x \\ \sigma_y \\ \tau_{xy} \end{Bmatrix}(z) dz; \\
\begin{Bmatrix} Q_x \\ Q_y \end{Bmatrix} &= \int_{-\frac{h}{2}}^{\frac{h}{2}} f(z) \begin{Bmatrix} \tau_{xz} \\ \tau_{yz} \end{Bmatrix} dz = \sum_{k=1}^n \int_{z_k}^{z_{k+1}} f(z) \begin{Bmatrix} \tau_{xz} \\ \tau_{yz} \end{Bmatrix} dz
\end{aligned} \tag{12}$$

Or, in terms of strains, by using Eqs. (2)-(3) and (8), we get :

$$\begin{aligned}
\begin{Bmatrix} N_x \\ N_y \\ N_{xy} \end{Bmatrix} &= \sum_{k=1}^n \left\{ \int_{z_k}^{z_{k+1}} \left[\bar{C}_b \right]^{(k)} \begin{Bmatrix} \varepsilon_x^0 \\ \varepsilon_y^0 \\ \gamma_{xy}^0 \end{Bmatrix} dz + \int_{z_k}^{z_{k+1}} \left[\bar{C}_b \right]^{(k)} \begin{Bmatrix} \kappa_x \\ \kappa_y \\ \gamma_{xy} \end{Bmatrix}(z) dz \right\} \\
\begin{Bmatrix} M_x \\ M_y \\ M_{xy} \end{Bmatrix} &= \sum_{k=1}^n \left\{ \int_{z_k}^{z_{k+1}} \left[\bar{C}_b \right]^{(k)} \begin{Bmatrix} \varepsilon_x^0 \\ \varepsilon_y^0 \\ \gamma_{xy}^0 \end{Bmatrix}(z) dz + \int_{z_k}^{z_{k+1}} \left[\bar{C}_b \right]^{(k)} \begin{Bmatrix} \kappa_x \\ \kappa_y \\ \gamma_{xy} \end{Bmatrix}(z^2) dz \right\} \\
\begin{Bmatrix} Q_x \\ Q_y \end{Bmatrix} &= \sum_{k=1}^n \left\{ \int_{z_k}^{z_{k+1}} \left[\bar{C}_s \right]^{(k)} \begin{Bmatrix} \gamma_{xz} \\ \gamma_{yz} \end{Bmatrix} f(z) dz \right\} = \sum_{k=1}^n \left\{ \int_{z_k}^{z_{k+1}} \left[\bar{C}_s \right]^{(k)} f^2(z) \begin{Bmatrix} \gamma_{xz}^0 \\ \gamma_{yz}^0 \end{Bmatrix} dz \right\}
\end{aligned} \tag{13}$$

The Eq. (13) may be written in the form :

$$\begin{aligned}
\{N\} &= [A]\{\varepsilon^0\} + [B]\{\kappa\} \\
\{M\} &= [B]\{\varepsilon^0\} + [D]\{\kappa\} \\
\{Q\} &= [S]\{\gamma^0\}
\end{aligned} \tag{14}$$

In matrix form, the stress resultants-strains relationship is given by:

$$\begin{Bmatrix} N \\ M \\ Q \end{Bmatrix} = \begin{bmatrix} A & B & 0 \\ B & D & 0 \\ 0 & 0 & S \end{bmatrix} \begin{Bmatrix} \varepsilon^0 \\ \kappa \\ \gamma^0 \end{Bmatrix} \tag{15}$$

Where

$$N = \{N_x \ N_y \ N_{xy}\}^T, M = \{M_x \ M_y \ M_{xy}\}^T, Q = \{Q_x \ Q_y\}^T \tag{16a}$$

$$\varepsilon^0 = \{\varepsilon_x^0 \ \varepsilon_y^0 \ \gamma_{xy}^0\}^T, \kappa = \{\kappa_x \ \kappa_y \ \kappa_{xy}\}^T, \gamma^0 = \{\gamma_{xz}^0 \ \gamma_{yz}^0\}^T \tag{16b}$$

For a composite plate comprising n orthotropic laminae, the constitutive stiffness matrices $[A]$, $[B]$, $[D]$ and $[S]$, representing membrane, coupling, bending, and shear effects, respectively, are formulated as follows:

$$A = \begin{bmatrix} A_{11} & A_{12} & A_{16} \\ A_{21} & A_{22} & A_{26} \\ A_{61} & A_{62} & A_{66} \end{bmatrix}; B = \begin{bmatrix} B_{11} & B_{12} & B_{16} \\ B_{21} & B_{22} & B_{26} \\ B_{61} & B_{62} & B_{66} \end{bmatrix}; D = \begin{bmatrix} D_{11} & D_{12} & D_{16} \\ D_{21} & D_{22} & D_{26} \\ D_{61} & D_{62} & D_{66} \end{bmatrix}; S = \begin{bmatrix} S_{44} & S_{45} \\ S_{54} & S_{55} \end{bmatrix} \tag{17}$$

The expressions for the stiffness components are as follows [71]:

$$\begin{pmatrix} A_{ij} & B_{ij} & D_{ij} \end{pmatrix} = \int_{-h/2}^{h/2} \left[\overline{C}_b \right]_{ij}^{(k)} (1, z, z^2) dz; (i, j) = (1, 2, 6) \quad (18a)$$

$$S_{ij} = \int_{-h/2}^{h/2} \left[\overline{C}_s \right]_{ij}^{(k)} [f(z)]^2 dz; (i, j) = (4, 5) \quad (18b)$$

2. Formulate finite element

The proposed element, HSBQLP20, is first developed using the strain approach and TrSDPT. As shown in Fig. 4, this element possesses five Dofs per node: three translational displacements (u, v, w) along the x, y and z axes, respectively, and two rotational degrees of freedom (β_x, β_y) in respectively the $z-y$ and $z-x$ planes.

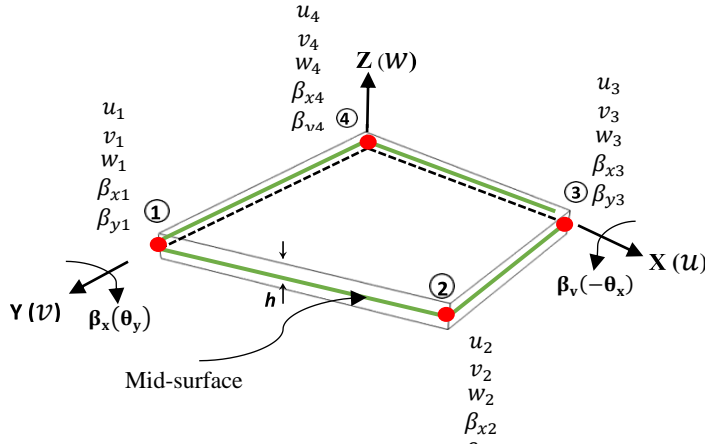


Figure 4. High-Order Strain-Based Quadrilateral Laminated Plate HSBQLP20.

3.1 Displacements field of the (HSBQLP20) element

To construct the displacement field of the proposed element (HSBQLP20), the present study integrates the displacement formulations of the plate element (SBQMP) developed by Bellounar et al. [63] and the membrane element (SBRIE) proposed by Sabir and Sfendji [56].

3.1.1 The displacement fields for the membrane element (SBRIE)

The obtained displacement field is given by supposing Eq (4) equal to zero and performing the integration [56]:

$$u_0 = \alpha_1 - \alpha_3 y, v_0 = \alpha_2 + \alpha_3 x \quad (19)$$

After using three constants $\{\alpha_1, \alpha_2, \alpha_3\}$ to represent the rigid body motion components, five constants $\{\alpha_4, \alpha_5, \dots, \alpha_8\}$ remain to describe the deformation of the element. These constants are distributed among the different deformation modes as follows [56]:

$$\begin{aligned} \varepsilon_x &= \alpha_4 + \alpha_5 y \\ \varepsilon_y &= \alpha_6 + \alpha_7 x \\ \gamma_{xy} &= \alpha_8 \end{aligned} \quad (20)$$

The strains defined by Eq. (20) satisfy the compatibility equation (21) given below [56]:

$$\begin{aligned} \frac{\partial^2 \varepsilon_x}{\partial y^2} + \frac{\partial^2 \varepsilon_y}{\partial x^2} - \frac{\partial^2 \varepsilon_{xy}}{\partial x \partial y} &= 0 \\ \frac{\partial^2 (\alpha_4 + \alpha_5 y)}{\partial y^2} + \frac{\partial^2 (\alpha_6 + \alpha_7 x)}{\partial x^2} - \frac{\partial^2 (\alpha_8)}{\partial x \partial y} &= 0 \end{aligned} \quad (21)$$

The expressions given by Eqs. (20) are then transformed in terms of u_0 and v_0 according to Eq. (4).

The resulting equations are subsequently integrated to yield :

$$\begin{aligned} u_0 &= \alpha_4 x + \alpha_5 x y - \alpha_7 \frac{y^2}{2} + \alpha_8 \frac{y}{2} \\ v_0 &= -\alpha_5 \frac{x^2}{2} + y \alpha_6 + x y \alpha_7 + \frac{x}{2} \alpha_8 \end{aligned} \quad (22)$$

The final displacement functions are obtained by adding Eqs. (19) and (22), which yields the following expressions [56] :

$$\begin{aligned} u_0 &= \alpha_1 - \alpha_3 y + \alpha_4 x + \alpha_5 x y - \alpha_7 \frac{y^2}{2} + \alpha_8 \frac{y}{2} \\ v_0 &= \alpha_2 + \alpha_3 x - \alpha_5 \frac{x^2}{2} + y \alpha_6 + x y \alpha_7 + \frac{x}{2} \alpha_8 \end{aligned} \quad (23)$$

In matrix form :

$$\begin{Bmatrix} u_0 \\ v_0 \end{Bmatrix} = [P_m] \{ \alpha_m \} \quad (24)$$

Where $\{ \alpha_m \} = \{ \alpha_1, \alpha_2, \dots, \alpha_8 \}^T$

$$[P_m] = \begin{bmatrix} 1 & 0 & -y & x & x y & 0 & -\frac{y^2}{2} & \frac{y}{2} \\ 0 & 1 & x & 0 & -\frac{x^2}{2} & y & x y & \frac{x}{2} \end{bmatrix} \quad (25)$$

3.1.2 The displacement fields for the bending element (SBQMP)

The same procedure used for the membrane element (SBRIE) is applied to establish the displacement fields of the bending element (SBQMP).

Similar to the membrane element, three constants $\{ \alpha_1, \alpha_2, \alpha_3 \}$ are introduced to represent the rigid body motion [63]:

$$w_0 = \alpha_9 - \alpha_{10} x - \alpha_{11} y, \beta_x = \alpha_{10}, \beta_y = \alpha_{11} \quad (26)$$

while the remaining constants $\{ \alpha_{12}, \alpha_{13}, \dots, \alpha_{20} \}$ are associated with the element's deformation modes. These constants correspond to bending and twisting deformation components[63] :

$$\begin{aligned} \kappa_x &= \alpha_{12} + \alpha_{13} y + \alpha_{15} \frac{x}{2} \\ \kappa_y &= \alpha_{13} \frac{y}{2} + \alpha_{14} + \alpha_{15} x \\ \kappa_{xy} &= 2\alpha_{13} x + 2\alpha_{15} y + \alpha_{16} \\ \gamma_{xz} &= \alpha_{17} + \alpha_{18} y \\ \gamma_{yz} &= \alpha_{19} + \alpha_{20} y \end{aligned} \quad (27)$$

The application of the compatibility equations ensures that the derived strain components satisfy the conditions of strain continuity throughout the element domain. The compatibility relations are expressed as follows[63]:

$$\begin{aligned}\frac{\partial^2 \kappa_x}{\partial y^2} + \frac{\partial^2 \kappa_y}{\partial x^2} &= \frac{\partial^2 \kappa_{xy}}{\partial x \partial y} \\ \frac{\partial^2 \gamma_{xz}}{\partial x \partial y} - \frac{\partial^2 \gamma_{yz}}{\partial x^2} + \frac{\partial \kappa_{xy}}{\partial x} &= 2 \frac{\partial \kappa_x}{\partial y} \\ \frac{\partial^2 \gamma_{yz}}{\partial x \partial y} - \frac{\partial^2 \gamma_{xz}}{\partial y^2} + \frac{\partial \kappa_{xy}}{\partial y} &= 2 \frac{\partial \kappa_y}{\partial x}\end{aligned}\quad (28)$$

Substituting the assumed forms of the strain components into the above equations :

$$\begin{aligned}\frac{\partial^2 \left(\alpha_{12} + \alpha_{13}y + \alpha_{15} \frac{x}{2} \right)}{\partial y^2} + \frac{\partial^2 \left(\alpha_{13} \frac{y}{2} + \alpha_{14} + \alpha_{15}x \right)}{\partial x^2} &= \frac{\partial^2 (2\alpha_{13}x + 2\alpha_{15}y + \alpha_{16})}{\partial x \partial y} = \frac{\partial^2 \kappa_{xy}}{\partial x \partial y} \\ \frac{\partial^2 (\alpha_{17} + \alpha_{18}y)}{\partial x \partial y} - \frac{\partial^2 (\alpha_{19} + \alpha_{20}y)}{\partial x^2} + \frac{\partial (2\alpha_{13}x + 2\alpha_{15}y + \alpha_{16})}{\partial x} &= 2\alpha_{13} = 2 \frac{\partial \kappa_x}{\partial y} \\ \frac{\partial^2 (\alpha_{19} + \alpha_{20}y)}{\partial x \partial y} - \frac{\partial^2 (\alpha_{17} + \alpha_{18}y)}{\partial y^2} + \frac{\partial^2 (2\alpha_{13}x + 2\alpha_{15}y + \alpha_{16})}{\partial y} &= 2\alpha_{15} = 2 \frac{\partial \kappa_y}{\partial x}\end{aligned}\quad (29)$$

The expressions given by Eqs. (27) are then transformed in terms of w_0 and β_x , β_y according to Eq. (4). The resulting equations are subsequently integrated to yield :

$$\begin{aligned}w_0 &= -\left(\frac{x^2}{2}\right)\alpha_{12} - \left(\frac{x^2y}{2} + \frac{y^3}{12}\right)\alpha_{13} - \left(\frac{y^2}{2}\right)\alpha_{14} - \left(\frac{xy^2}{2} + \frac{x^3}{12}\right)\alpha_{15} - \alpha_{16} \frac{xy}{2} + \alpha_{17} \frac{x}{2} + \alpha_{18} \frac{xy}{2} + \alpha_{19} \frac{y}{2} + \alpha_{20} \frac{xy}{2} \\ \beta_x &= x\alpha_{12} + xy\alpha_{13} + \left(\frac{y^2}{2} + \frac{x^2}{4}\right)\alpha_{15} + \frac{y}{2}\alpha_{16} + \frac{1}{2}\alpha_{17} + \frac{y}{2}\alpha_{18} - \frac{y}{2}\alpha_{20} \\ \beta_y &= \left(\frac{x^2}{2} + \frac{y^2}{4}\right)\alpha_{13} + y\alpha_{14} + xy\alpha_{15} + \frac{x}{2}\alpha_{16} - \frac{x}{2}\alpha_{18} + \frac{1}{2}\alpha_{19} + \frac{x}{2}\alpha_{20}\end{aligned}\quad (30)$$

The final displacement functions are obtained by adding Eqs. (26) and (30), which yields the following expressions [63] :

$$\begin{aligned}w_0 &= \alpha_9 - \alpha_{10}x - \alpha_{11}y - \left(\frac{x^2}{2}\right)\alpha_{12} - \left(\frac{x^2y}{2} + \frac{y^3}{12}\right)\alpha_{13} - \left(\frac{y^2}{2}\right)\alpha_{14} - \left(\frac{xy^2}{2} + \frac{x^3}{12}\right)\alpha_{15} - \alpha_{16} \frac{xy}{2} + \alpha_{17} \frac{x}{2} + \alpha_{18} \frac{xy}{2} + \alpha_{19} \frac{y}{2} + \alpha_{20} \frac{xy}{2} \\ \beta_x &= \alpha_{10} + x\alpha_{12} + xy\alpha_{13} + \left(\frac{y^2}{2} + \frac{x^2}{4}\right)\alpha_{15} + \frac{y}{2}\alpha_{16} + \frac{1}{2}\alpha_{17} + \frac{y}{2}\alpha_{18} - \frac{y}{2}\alpha_{20} \\ \beta_y &= \alpha_{11} + \left(\frac{x^2}{2} + \frac{y^2}{4}\right)\alpha_{13} + y\alpha_{14} + xy\alpha_{15} + \frac{x}{2}\alpha_{16} - \frac{x}{2}\alpha_{18} + \frac{1}{2}\alpha_{19} + \frac{x}{2}\alpha_{20}\end{aligned}\quad (31)$$

In matrix form :

$$\begin{Bmatrix} w \\ \beta_x \\ \beta_y \end{Bmatrix} = [P_b]\{\alpha_b\} \quad (32)$$

Where $\{\alpha_b\} = \{\alpha_9, \alpha_2, \dots, \alpha_{20}\}^T$

$$[\mathbf{P}_b] = \begin{bmatrix} 1 & -x & -y & -\frac{x^2}{2} & -\left(\frac{x^2y}{2} + \frac{y^3}{12}\right) & -\frac{y^2}{2} & -\left(\frac{xy^2}{2} + \frac{x^3}{12}\right) & -\frac{xy}{2} & \frac{x}{2} & \frac{xy}{2} & \frac{y}{2} & \frac{xy}{2} \\ 0 & 1 & 0 & x & xy & 0 & \left(\frac{y^2}{2} + \frac{x^2}{4}\right) & \frac{y}{2} & \frac{1}{2} & \frac{y}{2} & 0 & -\frac{y}{2} \\ 0 & 0 & 1 & 0 & \left(\frac{x^2}{2} + \frac{y^2}{4}\right) & y & xy & \frac{x}{2} & 0 & -\frac{x}{2} & \frac{1}{2} & \frac{x}{2} \end{bmatrix} \quad (33)$$

As mentioned earlier, the displacement field of the present element (HSBQLP20) is obtained by combining Eq. (25) and Eq. (33). The resulting expressions can be expressed in terms of twenty constants, represented as $\{\alpha\}^T = \{\alpha_1, \alpha_2, \dots, \alpha_{20}\}$, as follows [72] :

$$\{\mathbf{U}_e\} = \begin{Bmatrix} \mathbf{U}_m \\ \mathbf{U}_b \end{Bmatrix} = \begin{Bmatrix} \mathbf{u}_0 \\ \mathbf{v}_0 \\ \mathbf{w}_0 \\ \beta_x \\ \beta_y \end{Bmatrix} = \begin{bmatrix} [\mathbf{P}_m]_{(2 \times 8)} & [\mathbf{0}]_{(2 \times 12)} \\ [\mathbf{0}]_{(3 \times 8)} & [\mathbf{P}_b]_{(3 \times 12)} \end{bmatrix} \begin{Bmatrix} \{\alpha_m\} \\ \{\alpha_b\} \end{Bmatrix} = [\mathbf{P}]\{\alpha\} \quad (34)$$

Where

$$[\mathbf{P}] = \begin{bmatrix} 1 & 0 & -y & x & xy & 0 & -\frac{y^2}{2} & \frac{y}{2} & 0 & 0 & 0 & 0 & 0 & 0 & 0 & 0 & 0 & 0 & 0 & 0 & 0 \\ 0 & 1 & x & 0 & -\frac{x^2}{2} & y & xy & \frac{x}{2} & 0 & 0 & 0 & 0 & 0 & 0 & 0 & 0 & 0 & 0 & 0 & 0 & 0 & 0 \\ 0 & 0 & 0 & 0 & 0 & 0 & 0 & 1 & -x & -y & -\frac{x^2}{2} & -\left(\frac{x^2y}{2} + \frac{y^3}{12}\right) & -\frac{y^2}{2} & -\left(\frac{xy^2}{2} + \frac{x^3}{12}\right) & -\frac{xy}{2} & \frac{x}{2} & \frac{xy}{2} & \frac{y}{2} & \frac{xy}{2} \\ 0 & 0 & 0 & 0 & 0 & 0 & 0 & 0 & 0 & 1 & 0 & x & xy & 0 & \left(\frac{y^2}{2} + \frac{x^2}{4}\right) & \frac{y}{2} & \frac{1}{2} & \frac{y}{2} & 0 & -\frac{y}{2} \\ 0 & 0 & 0 & 0 & 0 & 0 & 0 & 0 & 0 & 0 & 0 & 1 & 0 & \left(\frac{x^2}{2} + \frac{y^2}{4}\right) & y & xy & \frac{x}{2} & 0 & -\frac{x}{2} & \frac{1}{2} & \frac{x}{2} \end{bmatrix}$$

The transformation matrix $[R]$, which connects the vector of elemental nodal displacements for $\{\delta_e\}^T = (u_1, v_1, w_1, \beta_{x1}, \beta_{y1}, \dots, u_4, v_4, w_4, \beta_{x4}, \beta_{y4})$ to the vector of constants $\{\alpha\}^T = (\alpha_1, \alpha_2, \dots, \alpha_{20})$, can be represented in the form of a matrix by the following formula:

$$\{\delta_e\} = [R]\{\alpha\} \quad (35)$$

Where

$$[R] = \begin{bmatrix} [P_1] & [P_2] & [P_3] & [P_4] \end{bmatrix}^T \quad (36)$$

The matrices $[P_i]$ (corresponding to x_i and y_i for node i , where $i = 1, 2, 3$, and 4) are defined by the expression given in Eq. (34) :

$$[P_i] = \begin{bmatrix} [\mathbf{P}_m]_i & \mathbf{0} \\ \mathbf{0} & [\mathbf{P}_b]_i \end{bmatrix} \quad (37)$$

Now, by using Eq. (35), we can derive the vector of constant values $\{\alpha\}$.

$$\{\alpha\} = [R]^{-1}\{\delta_e\} \quad (38)$$

Next, by replacing Eq. (38) in Eq. (34), we have:

$$\{U_e\} = [P][R]^{-1}\{\delta_e\} = [N]\{\delta_e\} \quad (39)$$

Where

$$[N] = [P][R]^{-1} \quad (40)$$

3.2 Strain–displacement relations

The membrane strains $\{\varepsilon_m\}$ are evaluated using Eq. (4) as follow :

$$\{\varepsilon^0\} = \begin{Bmatrix} \varepsilon_x^0 \\ \varepsilon_y^0 \\ \gamma_{xy}^0 \end{Bmatrix} = \begin{bmatrix} \frac{\partial}{\partial x} & 0 & 0 \\ 0 & \frac{\partial}{\partial y} & 0 \\ \frac{\partial}{\partial y} & \frac{\partial}{\partial x} & 0 \end{bmatrix} \begin{Bmatrix} u_0 \\ v_0 \end{Bmatrix} = [G_m] \{\alpha\} \quad (41)$$

By substituting Eq. (34) into Eq. (41), we obtain :

$$\{\varepsilon^0\} = \begin{Bmatrix} \varepsilon_x^0 \\ \varepsilon_y^0 \\ \gamma_{xy}^0 \end{Bmatrix} = \begin{bmatrix} \frac{\partial}{\partial x} & 0 & 0 \\ 0 & \frac{\partial}{\partial y} & 0 \\ \frac{\partial}{\partial y} & \frac{\partial}{\partial x} & 0 \end{bmatrix} \{[P_m]_{3 \times 8} [0]_{3 \times 12}\} \{\alpha\} = [G_m]_{3 \times 20} \{\alpha\} \quad (42)$$

Using Eq. (4), the relationships between curvatures, shear strains, and displacements are expressed as follows :

$$\{\kappa\} = \begin{Bmatrix} \kappa_x \\ \kappa_y \\ \kappa_{xy} \end{Bmatrix} = \begin{bmatrix} 0 & \frac{\partial}{\partial x} & 0 \\ 0 & 0 & \frac{\partial}{\partial y} \\ 0 & \frac{\partial}{\partial y} & \frac{\partial}{\partial x} \end{bmatrix} \{[0]_{3 \times 8} [P_b]_{3 \times 12}\} \{\alpha\} = [G_b]_{3 \times 20} \{\alpha\} \quad (43)$$

$$\{\gamma\} = \begin{Bmatrix} \gamma_{xz} \\ \gamma_{yz} \end{Bmatrix} = \begin{bmatrix} \frac{\partial}{\partial x} & 1 & 0 \\ \frac{\partial}{\partial y} & 0 & 1 \end{bmatrix} \{[0]_{3 \times 8} [P_b]_{3 \times 12}\} \{\alpha\} = [G_s]_{2 \times 20} \{\alpha\} \quad (44)$$

Where the membrane $[G_m]$, bending $[G_b]$, and transverse shear $[G_s]$ strain matrices are defined as follows[72] :

$$[G_m] = \begin{bmatrix} 0 & 0 & 0 & 1 & y & 0 & 0 & 0 & 0 & 0 & 0 & 0 & 0 & 0 & 0 & 0 & 0 & 0 & 0 & 0 \\ 0 & 0 & 0 & 0 & 0 & 1 & x & 0 & 0 & 0 & 0 & 0 & 0 & 0 & 0 & 0 & 0 & 0 & 0 & 0 \\ 0 & 0 & 0 & 0 & 0 & 0 & 0 & 1 & 0 & 0 & 0 & 0 & 0 & 0 & 0 & 0 & 0 & 0 & 0 & 0 \end{bmatrix} \quad (45)$$

$$[G_b] = \begin{bmatrix} 0 & 0 & 0 & 0 & 0 & 0 & 0 & 0 & 0 & 0 & 0 & 1 & y & 0 & \frac{x}{2} & 0 & 0 & 0 & 0 & 0 \\ 0 & 0 & 0 & 0 & 0 & 0 & 0 & 0 & 0 & 0 & 0 & 0 & 0 & \frac{y}{2} & 1 & x & 0 & 0 & 0 & 0 & 0 \\ 0 & 0 & 0 & 0 & 0 & 0 & 0 & 0 & 0 & 0 & 0 & 0 & 0 & 2x & 0 & 2y & 1 & 0 & 0 & 0 & 0 \end{bmatrix} \quad (46)$$

$$[G_s] = \begin{bmatrix} 0 & 0 & 0 & 0 & 0 & 0 & 0 & 0 & 0 & 0 & 0 & 0 & 0 & 0 & 0 & 0 & 1 & y & 0 & 0 \\ 0 & 0 & 0 & 0 & 0 & 0 & 0 & 0 & 0 & 0 & 0 & 0 & 0 & 0 & 0 & 0 & 0 & 0 & 1 & x \end{bmatrix} \quad (47)$$

The relationship between displacements and strains can be derived by substituting Eq. (38) into Eqs. (42) - (44), giving [72,73]:

$$\{\varepsilon^0\} = [G_m][R]^{-1}\{\delta_e\} = [B_m]\{\delta_e\} \quad (48)$$

$$\{\kappa\} = [G_b][R]^{-1}\{\delta_e\} = [B_b]\{\delta_e\} \quad (49)$$

$$\{\gamma\} = [G_s][R]^{-1}\{\delta_e\} = [B_s]\{\delta_e\} \quad (50)$$

where $[B_m]$, $[B_b]$, and $[B_s]$ represent strain-displacement matrices defined by:

$$[B_m] = [G_m][R]^{-1}; [B_b] = [G_b][R]^{-1}; [B_s] = [G_s][R]^{-1} \quad (51)$$

3.3 Derivation of elemental matrices

3.3.1 Static analysis

The stiffness matrix is derived by applying the principle of total potential energy:

$$\pi = U - W \quad (51)$$

where U and W denote the strain energy and the work done by external loads, respectively.

The expression for the strain energy potential is given by Tati [65] as follows:

$$U = \frac{1}{2} \int_V (\{\varepsilon\}^T \{\sigma\} + \{\gamma\}^T \{\tau\}) dV = \frac{1}{2} \int_V (\{\varepsilon^0\}^T \{\sigma\} + z \{\kappa\}^T \{\sigma\} + \{\gamma\}^T \{\tau\}) dV \quad (52)$$

By integrating through the thickness and applying Eqs. (12) and (13), Eq. (53) becomes [64]:

$$U = \frac{1}{2} \int_S (\{\varepsilon^0\}^T \{N\} + \{\kappa\}^T \{M\} + \{\gamma\}^T \{Q\}) dS \quad (53)$$

By substituting Eqs. (15), (48), (49), and (50) into the above equation, we obtain:

$$U = \frac{1}{2} \int_S \left[\{\delta_e\}^T \left([B_m]^T [A] [B_m] + [B_m]^T [B] [B_b] + [B_b]^T [B] [B_m] \right. \right. \\ \left. \left. + [B_b]^T [D] [B_b] + [B_s]^T [S] [B_s] \right) \{\delta_e\} \right] dS \quad (54)$$

Where Ω and V represent the top surface and the volume of the plate, respectively.

The external work generated by the applied distributed load $q(x, y)$ on the FGM plate is expressed by as follows [65] :

$$(55)$$

$$W = \int_S w_0 \times q(x, y) dS$$

By substituting Eq. (40) into Eq. (55), we obtain:

$$W = \int_S \{\delta_e\}^T [N]^T \times q(x, y) dS \quad (56)$$

Substituting Eqs. (54) and (56) into Eq. (51) yields:

$$\begin{aligned} \pi = U &= \frac{1}{2} \int_S \left[\{\delta_e\}^T \left(\begin{array}{l} [B_m]^T [A][B_m] + [B_m]^T [B][B_b] + [B_b]^T [B][B_m] \\ + [B_b]^T [D][B_b] + [B_s]^T [S][B_s] \end{array} \right) \{\delta_e\} \right] dS \\ &\quad - \int_S \{\delta_e\}^T [N]^T \times q(x, y) dS \end{aligned} \quad (57)$$

The equilibrium equation for linear bending analysis can be expressed as follows:

$$[K_e] \{\delta_e\} = \{F_e\} \quad (58)$$

where $[K^e]$ represents the element stiffness matrix, and $\{F^e\}$ denotes the corresponding nodal force vector for the element, given by :

$$[K_e] = \int_S \left([B_m]^T [A][B_m] + [B_b]^T [B][B_m] + [B_b]^T [D][B_b] + [B_s]^T [S][B_s] \right) dS \quad (59)$$

$$\{F_e\} = \int_S [N]^T \times q(x, y) dS \quad (60)$$

3.3.1 Free vibrational analysis

In order to obtain the mass matrix, the Hamilton principle is used[64] :

$$\delta \int_0^t [T - (U - W)] dt = 0 \quad (61)$$

where T represents the kinetic energy, as defined by [64] :

$$T = \frac{1}{2} \int_S \int_{-\frac{h}{2}}^{\frac{h}{2}} \rho(z) \left(\{\dot{U}_e\}^T \{\dot{U}_e\} dz \right) dS \quad (62)$$

Where $\{U_e\} = \{u, v, w, \beta_x, \beta_y\}^T$ is the displacement nodal vector and $\rho(z)$ if the density.

Substituting Eq. (39) into the above equation yields:

$$T = \frac{1}{2} \int_S \int_{-\frac{h}{2}}^{\frac{h}{2}} \rho(z) \left(\{\dot{\delta}_e\}^T [N]^T [N] \{\dot{\delta}_e\} dz \right) dS = \frac{1}{2} \{\dot{\delta}_e\}^T \left(\int_S \int_{-\frac{h}{2}}^{\frac{h}{2}} [N]^T \rho(z) [N] dz dS \right) \{\dot{\delta}_e\} \quad (63)$$

The element mass matrix $[M_e]$ can be computed by the following expression :

$$[M_e] = \int_S \int_{-\frac{h}{2}}^{\frac{h}{2}} [N]^T \rho(z) [N] dz dS = \int_S [N]^T [I_0] [N] dS \quad (64)$$

where $[I_0]$ is the surface inertia matrix (or “thickness-integral matrix”) defined by the zero-, first- and second-order mass moments [34] :

$$[I_0] = \begin{bmatrix} m_0 & 0 & 0 & 0 & 0 \\ 0 & m_0 & 0 & 0 & 0 \\ 0 & 0 & m_0 & 0 & 0 \\ 0 & 0 & 0 & m_2 & 0 \\ 0 & 0 & 0 & 0 & m_2 \end{bmatrix} \quad (65)$$

$$m_0 = \int_{-\frac{h}{2}}^{\frac{h}{2}} \rho dz = \rho h; m_1 = \int_{-\frac{h}{2}}^{\frac{h}{2}} \rho z dz = 0; m_2 = \int_{-\frac{h}{2}}^{\frac{h}{2}} \rho z^2 dz = \rho \frac{h^3}{12} \quad (66)$$

In the case of free vibration, where the work done by external forces (W) is null, the Hamilton’s principle expressed in Eq. (61) leads to the following dynamic equation of equilibrium for the system [64]:

$$\begin{aligned} [K_e]\{\delta^e\} + [M_e]\{\ddot{\delta}^e\} &= \{0\} \\ ([K_e] - \omega^2 [M_e])\{\delta^e\} &= 0 \end{aligned} \quad (67)$$

The element stiffness and mass matrices, $[K_e]$ and $[M_e]$, given in Eqs. (59) and (64), respectively, together with the equivalent nodal load vector $\{F_e\}$ from Eq. (60), are assembled to form the global stiffness matrix $[K]$, mass matrix $[M]$, and global load vector $\{F\}$ of the structure.

For the static behavior, we apply the equilibrium equation[72]:

$$[K]\{\delta^e\} = \{F\} \quad (68)$$

For the free vibrational behavior, we apply the dynamic equilibrium equation[72]:

$$([K] - \omega^2 [M]) = 0 \quad (69)$$

3. Numerical findings and discussion

This paper investigates the statically and free-vibrational behavior of square, skewed and elliptical laminated plates by analyzing full plates utilizing the developed finite element approach. The findings obtained are validated against several available analytically and numerically derived solutions. The impact of several plate parameters including the number of layers, aspect ratio, fiber orientation, and boundary conditions has been investigated. The characteristics of the materials used in this study are presented in Table 2. The following two types of constraints are taken into account:

- For simply supported boundaries (SSSS) :

$$(v = w = \beta_y = 0) \text{ at } x = 0, a$$

$$(u = w = \beta_x = 0) \text{ at } y = 0, b$$

▪ For clamped boundaries (CCCC) :

at $x = 0, a$ and $y = 0, b$

Table 2. Material properties of the composite laminate.

Properties	Material (M)						
	M ₁	M ₂	M ₃	M ₄	M ₅	M ₆	M ₇
E ₁₁ (Gpa)	25	3	10	20	30	40	2.45
E ₂₂ (Gpa)	01	01	01	01	01	01	01
G ₁₂ (Gpa)	0.5	0.6	0.6	0.6	0.6	0.6	0.48
G ₁₃ (Gpa)	0.5	0.6	0.6	0.6	0.6	0.6	0.48
G ₂₃ (Gpa)	0.2	0.5	0.5	0.5	0.5	0.5	0.2
v ₁₂ = v ₂₃ = v ₁₃	0.25	0.25	0.25	0.25	0.25	0.25	0.23
ρ	01	01	01	01	01	01	01

4.1 Static analysis of laminated plates

The effectiveness and performance of the proposed quadrilateral element for analyzing the static behavior of simply supported symmetric cross-ply plates have been validated through several numerical examples. The material model M1 is applied in this work and the findings are compared with published numerical and analytical studies. The plates are subjected to both uniform and sinusoidal load distributions (\bar{p}_0), as illustrated in [Figure 5](#), which is expressed by[37]:

$$\text{Uniformly distributed load (UDL)} : \bar{p}(x, y) = \bar{p}_0$$

$$\text{Sinusoidally distributed load (SDL)} : \bar{p}(x, y) = \bar{p}_0 \sin\left(\frac{\pi x}{a}\right) \sin\left(\frac{\pi y}{b}\right)$$

The normalized displacement and stresses are expressed as follows[31]:

$$\bar{w} = \frac{(100E_2h^3)}{p_0a^4} w\left(\frac{a}{2}, \frac{b}{2}, 0\right); \bar{\sigma}_x = \frac{(h^2)}{p_0b^2} \sigma_x\left(\frac{a}{2}, \frac{b}{2}, \frac{h}{2}\right); \bar{\sigma}_y = \frac{(h^2)}{p_0b^2} \sigma_y\left(\frac{a}{2}, \frac{b}{2}, \frac{h}{4}\right) \quad (70a)$$

$$\bar{\tau}_{xy} = \frac{(h^2)}{p_0b^2} \tau_{xy}\left(0, 0, \frac{h}{2}\right); \bar{\tau}_{xz} = \frac{(h)}{p_0b} \tau_{xz}\left(0, \frac{b}{2}, 0\right); \bar{\tau}_{yz} = \frac{(h)}{p_0b} \tau_{yz}\left(\frac{a}{2}, 0, 0\right) \quad (70b)$$

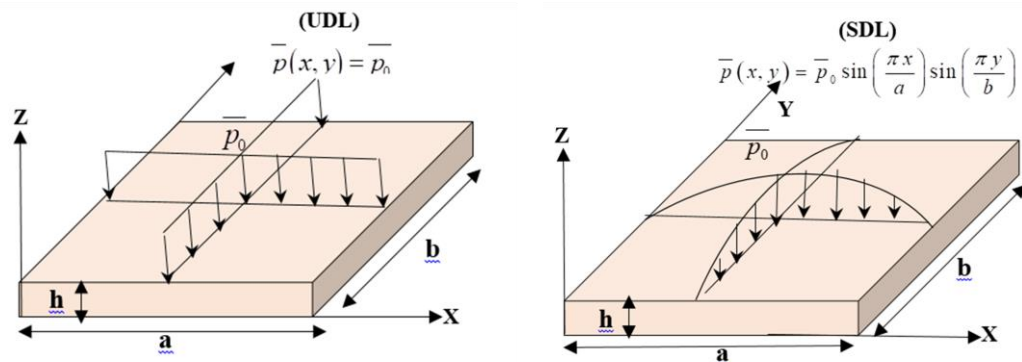


Figure 5. Square laminated plates subject to uniform and sinusoidal loading distributions.

4.1.1 Four layer [0°/90°/90°/0°] symmetric cross ply laminated plate subjected to sinusoidal loads

A four-layer symmetrical SSSS cross-ply laminate [0°/90°/90°/0°] exposed to a sinusoidal load as depicted in [Figure 5](#). For this example, material model M1 is chosen. Numerical values for dimensionless displacement and dimensionless stress with several ratio of thicknesses (a/h) using a mesh of 20×20 , are shown in [Table 3](#). These findings are comparable to other methods, such as the exact solution based on CPT by Pagano and Hatfield[74], the finite strip method (FSM) based on the HSDT by Akhras et al.[75], the inverse hyperbolic shear deformation theory (IHSDT) proposed by Neeraj Grover et al.[23], and the exact closed-form solution (CFS) based on the refined shear deformation theory (TSDT) by Reddy [12].

It is observed that the current solution gives the best performance for all a/h ratios. When compared with the CFS-TSDT of Reddy[12], the present element HSBQLP20 provides more accurate results. For moderately thick plates with $a/h = 10$, the current results for displacement, in-plane stress, and normalized lateral shear stress demonstrate better accuracy compared to those derived using HSDT [12], [74], [75]. For thinner plates ($a/h = 100$) there are no significant variations between the various solutions.

[Figs. 6](#) and [7](#) show the stress variations over the width the plate with $a/h=10$, using different theories. It is evident that the present distribution of in plan stress ($\bar{\sigma}_x$) and ($\bar{\sigma}_y$) aligns exactly with Reddy's HSDT[12], and the transverse shear stresses ($\bar{\tau}_{yz}$) are also accurately predicted when compared to Reddy's HSDT[12]. Furthermore, the lateral shear stresses are continuously applied to the inner laminar plies.

Table 3. Normalized deflections and stresses of the four-layer [0°/90°/90°/0°] laminated square plate exposed to SDL.

a/h	Theory	\bar{w}	$\bar{\sigma}_x$	$\bar{\sigma}_y$	$\bar{\tau}_{xy}$	$\bar{\tau}_{xz}$	$\bar{\tau}_{yz}$
10	Present	0.7153	0.5472	0.3896	0.0274	0.2646	0.1540
	Exact[74]	0.743	0.559	0.401	0.028	0.301	0.196
	Reddy[12]	0.7147	0.5456	0.3888	0.0268	0.2640	0.1531
	Akhras et al. [75]	0.7149	0.5589	0.3974	0.0273	0.2697	0.1568
	Neeraj Grover et al.[23]	0.7284	0.5578	0.3947	0.0275	0.3287	0.1761
20	Present	0.5066	0.5399	0.3049	0.0234	0.2831	0.124
	Exact[74]	0.517	0.543	0.308	0.023	0.328	0.156
	Reddy[12]	0.5060	0.5393	0.3043	0.0228	0.2825	0.1234
	Akhras et al. [75]	0.5061	0.5523	0.3110	0.0233	0.2883	0.1272
	Neeraj Grover et al.[23]	0.5102	0.5425	0.3064	0.023	0.3542	0.1412
100	Present	0.4345	0.5391	0.2711	0.0214	0.2910	0.1125
	Exact[74]	0.439	0.539	0.276	0.022	0.337	0.141
	Reddy[12]	0.4343	0.5387	0.2708	0.0213	0.2897	0.1117
	Akhras et al. [75]	0.4343	0.5507	0.2769	0.0217	0.2948	0.1180
	Neeraj Grover et al.[23]	0.4345	0.5388	0.2710	0.0214	0.3643	0.1271

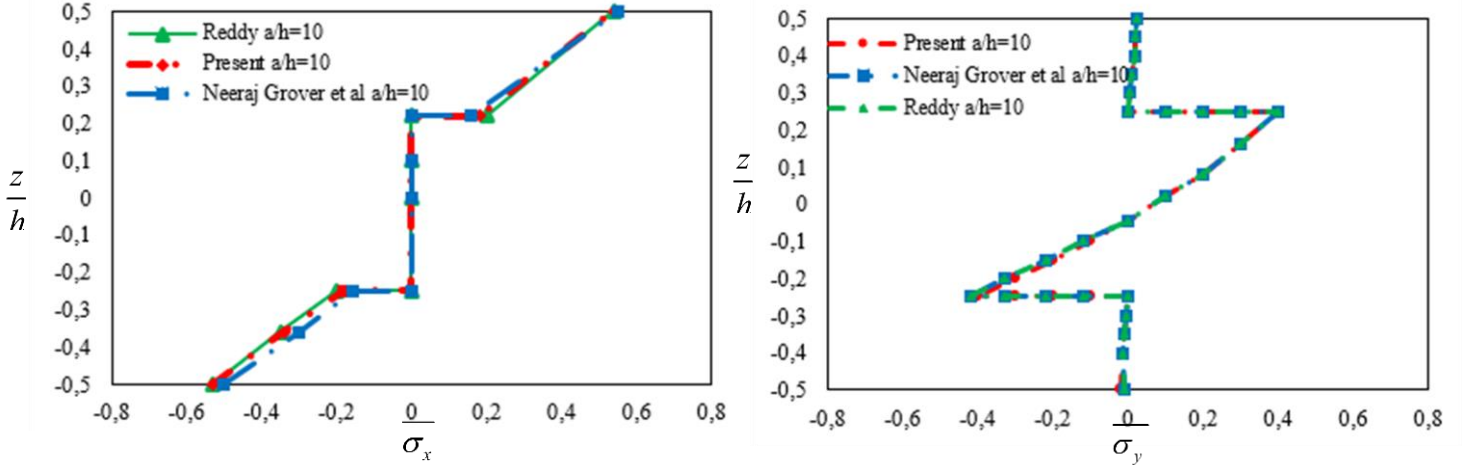


Figure 6. Variation of the normal and in plan stress, $\overline{\sigma}_x, \overline{\sigma}_y$ across thickness for $[0^\circ/90^\circ/90^\circ/0^\circ]$ laminated plate (M1) with $a/h=10$

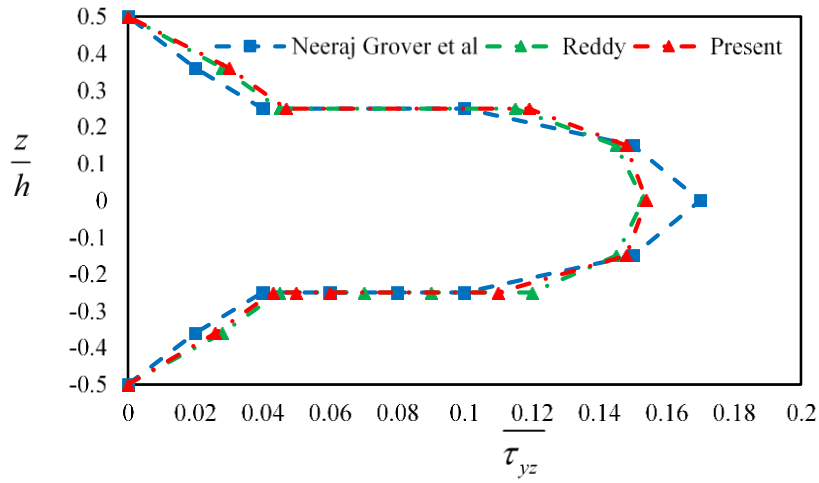


Figure 7. Variation of transverse shear stress, $\overline{\tau}_{yz}$ across thickness for $[0^\circ/90^\circ/90^\circ/0^\circ]$ laminated plate (M1) with $a/h=10$.

4.1.2 Symmetrical composite square plates subjected to UDL

Three simply supported, cross-laminated symmetric square plates made of material M1 (with length a and thickness h) are considered under UDL. A 12×12 mesh is employed for the analysis, as illustrated in Fig. 8.

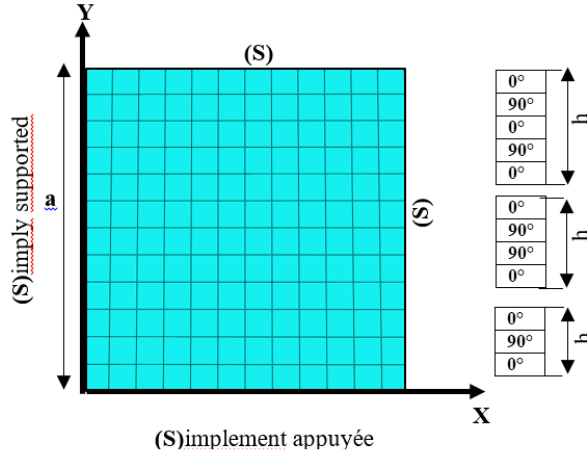


Figure 8. Geometry of a symmetrical cross-notched laminated composite plate and a type of mesh.

The convergence of the normalized central deflection (\bar{w}) as a function of different a/h ratios is presented in [Table 4](#) and [Fig. 9](#). The HSBQLP20 element yields numerical results that closely match Reddy's FSDT analytical solution [4]. It outperforms the FEM-Q4 [51] and DSG3 [51] elements in terms of accuracy and demonstrates comparable performance to more advanced elements such as ES-DSG [51], FEM-Q9 [51], and Bellounar's SBQLP [34]. Moreover, a shear-locking-free test is conducted for simply supported laminated square plates subjected to a uniform load, considering symmetric three-layer, and four-layer configurations. The numerical results of the normalized central deflection ($\bar{w} = w_c 100 E_2 h^3 / (q_0 a^4)$), obtained using a 20×20 mesh and for various side-to-thickness ratios (a/h), are presented in [Fig. 10](#). These results confirm that the SBQLP element remains free from shear locking and is insensitive to the length-to-thickness ratio, even for thin plates.

Table 4. Non-dimensionalized deflection (\bar{w}) of SSSS cross-laminated square plates exposed to UDL.

Theory	Layer	a / h		
		10	20	100
Present		0.9780	0.7463	0.6722
FEM-Q4 [51]		0.9874	0.7195	0.6307
FEM-Q9 [51]		1.0219	0.7573	0.6697
DSG3 [51]	[0°/90°/0°]	1.0159	0.7521	0.6642
ES-DSG3[51]		1.0287	0.7624	0.6743
SBQLP [34]		1.0218	0.7557	0.6677
Reddy [4]		1.0219	0.7572	0.6697
Present		1.0272	0.77025	0.6836
FEM-Q4 [51]		0.9883	0.7302	0.6430
FEM-Q9 [51]		1.0250	0.7694	0.6829
DSG3 [51]	[0°/90°/90°/0°]	1.0136	0.7604	0.6744
ES-DSG3[51]		1.0276	0.7716	0.6854
SBQLP [34]		1.0240	0.7671	0.6806
Reddy [4]		1.0250	0.7694	0.6833
Present		1.0270	0.7605	0.6882
FEM-Q4 [51]		0.9350	0.7182	0.6465
FEM-Q9 [51]		0.9727	0.7581	0.6868
DSG3 [51]	[0°/90°/0°/90°/0°]	0.9554	0.7404	0.6688
ES-DSG3[51]		0.9687	0.7515	0.6799
SBQLP [34]		0.9712	0.7555	0.6844
Reddy [4]		0.9727	0.7581	0.6874

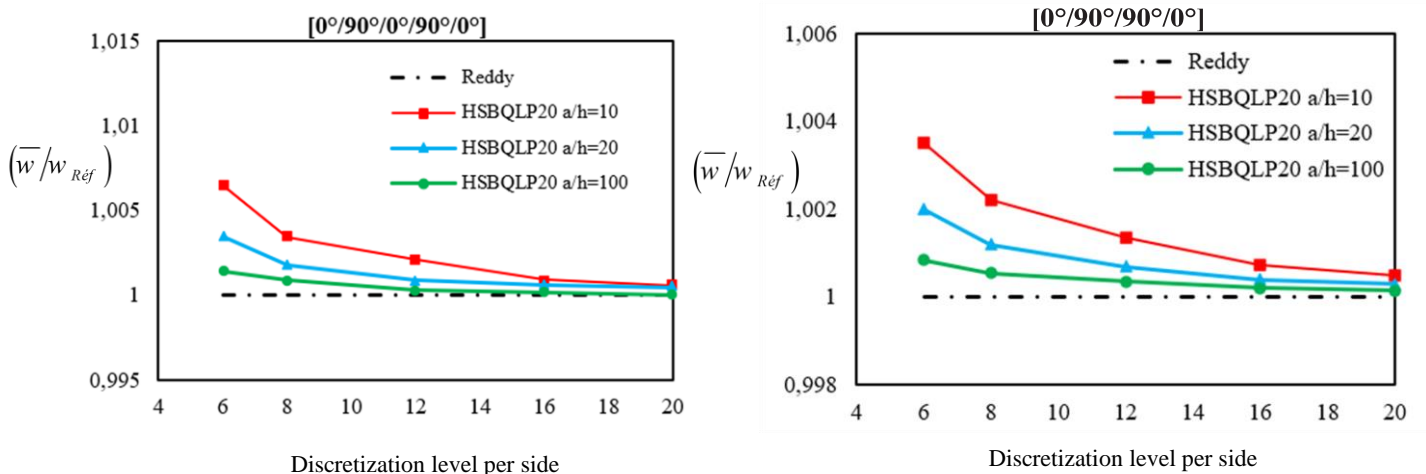


Figure 9. Convergent dimensiless deflection (\bar{w}) of cross-layered square composite plates subjected to UDL.

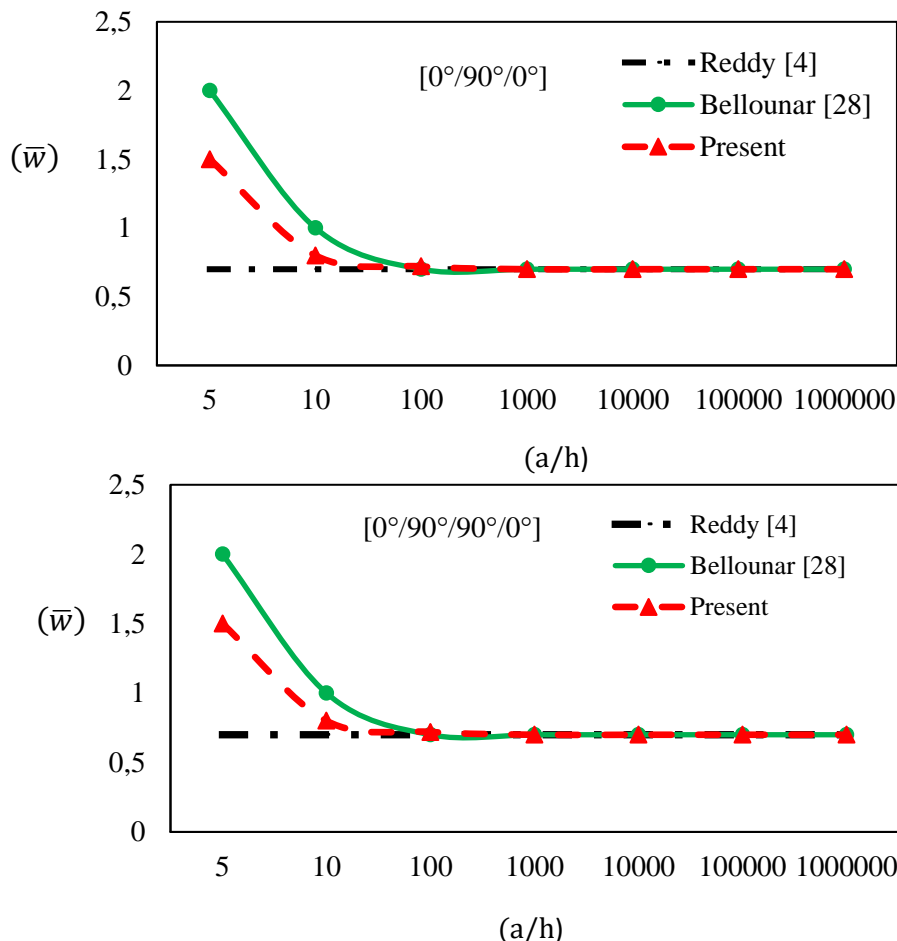


Figure 10. Dimensionless central deflection (\bar{w}) versus side-to-thickness ratio (a/h) for SSSS laminated square plates under uniform load, considering symmetric three-layer, and four-layer configurations.

4.1.3 Symmetric and anti-symmetric square Laminated Plates under Distorted Meshes

To demonstrate the applicability and accuracy of the proposed formulation in analyzing the normalized central deflection (\bar{w}) of composite laminated plates using both regular and distorted meshes. A simply supported square laminated plate of side length L with regular and distorted mesh patterns used in the analyses are shown in Fig. 11 is considered under a uniform transverse load using a $3 \times 3, 9 \times 9$, and 27×27 finite element mesh. The side-to-thickness ratio of the laminate is $L/h=10$. Two different stacking sequences are analyzed: a symmetric $[0^\circ/90^\circ/0^\circ]$ laminate and an antisymmetric $[0^\circ/90^\circ]$ laminate. All layers are of equal thickness and follow the mechanical properties of material model M1.

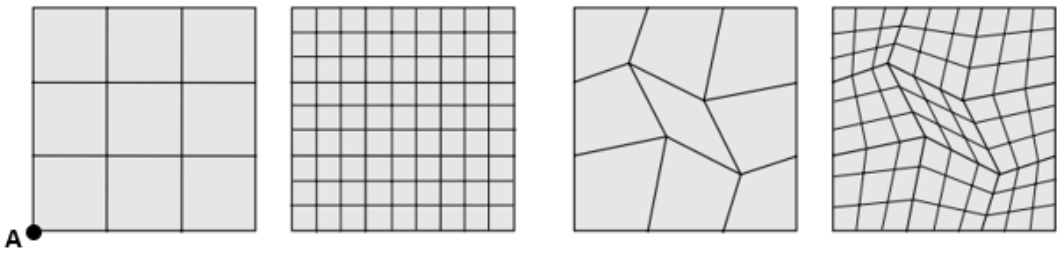


Figure 11. Regular and distorted mesh patterns.

The numerical results obtained using the present element are summarized in **Table 5**. An excellent agreement is observed with the analytical solution based on the First-Order Shear Deformation Theory (FSDT) by Reddy [4]. Moreover, the proposed element provides higher accuracy compared to the HQ4 element developed by Daghia et al. [76].

Table 5. Transverse displacement (\bar{w}) at point A for simply supported ($0^\circ/90^\circ$ and $0^\circ/90^\circ/0^\circ$) laminate subjected to uniform load

Theory	Stacking Sequence	$(\bar{w} = w_A 100 E_2 h^3 / (q_0 a^4))$		
		3x3	9x9	27x27
Present, distorted	[0°/90°]	1.95019	1.95065	1.95070
Reddy [4]		1.95058	1.95058	1.95058
HQ4, regular [76]		1.97191	1.95293	1.95084
HQ4, distorted [76]		1.96109	1.95077	1.95077
Present, distorted	[0°/90°/0°]	1.16710	1.16723	1.16760
Reddy [4]		1.16754	1.16754	1.16754
HQ4, regular [76]		1.17482	1.16831	1.16763
HQ4, distorted [76]		1.17610	1.16853	1.16765

4.2 Free vibrational analysis

This section presents some numerical applications to evaluate the performance of the HSBQLP20 element in the analysis of free vibrations of composite plates with varying geometries, aspect ratios, modulus ratios, angle of fiber orientation, as well as boundary conditions. In all examples, the material properties are assumed to be identical in all layers, while the fiber orientations may vary from layer to layer. The material characteristics of the different layers, which are applied in all plate types, are given in **Table 2**.

For convenience, the following nondimensional formulas are assumed :

$$\bar{\omega} = (\omega a^2 / \pi^2) \sqrt{\rho h / D_0} \quad \text{with} \quad D_0 = (E_2 h^3 / 12(1 - \nu_{12} \nu_{21})) \quad (71a)$$

$$\bar{\beta} = (\beta a^2 / h) \sqrt{\rho / E_2}; \bar{\Omega} = \Omega \sqrt{(h^2 \rho / E_2)}; \bar{\omega} = (\omega a^2 / \pi^2 h) \sqrt{\rho / E_2} \quad (71b)$$

4.2.1 Square laminated plates

4.2.1.1 Convergence Study

The convergence studies are carried out on a three-cross-layer [0°/90°/0°] square plate with clamped supported boundary conditions and multiple aspect ratio values ($a/h=5,10,20,100$) are studied with M6 material, the characteristics of which are given in [Table 2](#). The results of the five non-dimensional frequencies($\bar{\omega}$)of the present element HSBQLP20, and using four meshes (8×8 , 12×12 , 16×16 and 20×20) are shown in [Table 6](#), and the first six modes for the case with a length-to-thickness ratio of $l/h = 10$ are illustrated in [Fig. 12](#). The numerical results have been validated with the findings of Liew [77], which are based on FSDT, as well as with the smoothed FEM (ES-DSG3, MISQ20) developed by Nguyen-Van et al. [47] and Phan-Dao et al. [51], and the strain-based approach (SBQLP) of Belounar et al. [34], which is also based on FSDT.

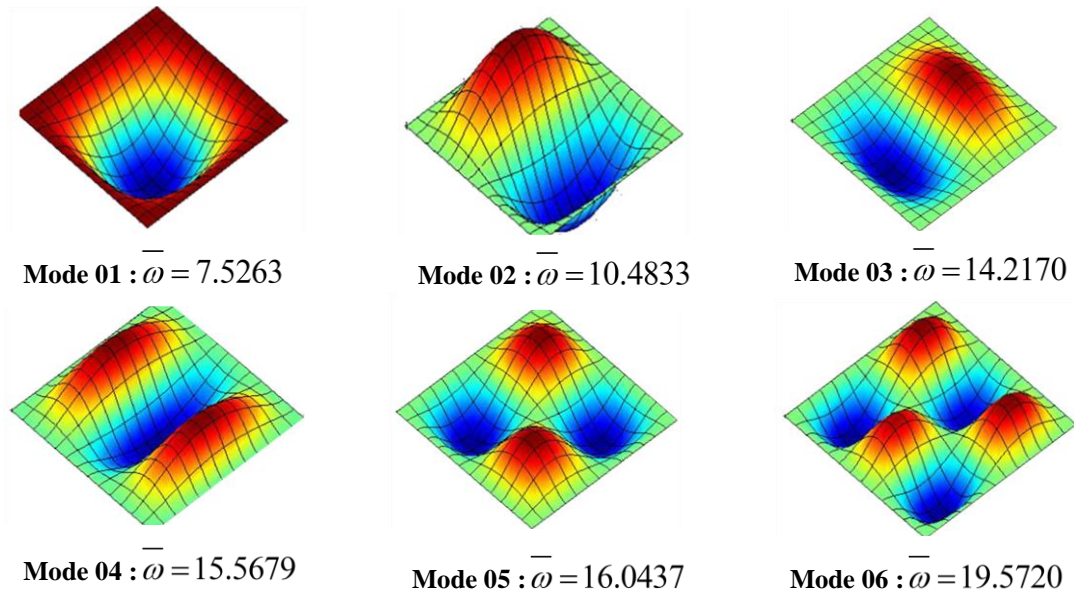


Figure 12. The first six eigenmode shapes of a three-ply [0°/90°/0°] CCCC square plate ($a/h = 10$)

Table 6 Non-dimensional natural frequencies ($\bar{\omega}$) of clamped cross-laminated square plates with various length-to-thickness ratio.

a/h	Theory	Modes				
		1	2	3	4	5
5	HSBQLP20 (8×8)	4.5476	6.8225	8.0183	9.4949	10.2620
	HSBQLP20 (12 × 12)	4.5239	6.7234	7.92430	9.3777	9.9373
	HSBQLP20 (16×16)	4.5159	6.6902	7.8918	9.3376	9.8282
	HSBQLP20 (20 × 20)	4.5123	6.6751	7.8768	9.3193	9.7785
	SBQLP (20 × 20) [34]	4. 4519	6. 6665	7. 7235	9. 2113	9. 8215
	p-Ritz (Liew) [77]	4. 447	6. 642	7. 700	9. 185	9. 738
	MISQ20 [47]	4. 4671	6. 7365	7. 7706	8. 7678	9. 2988
	HSBQLP20 (8×8)	7.5521	10.7018	14.4007	16.1785	16.5229
	HSBQLP20 (12 × 12)	7.5343	10.5495	14.2788	15.8639	16.0798
	HSBQLP20 (16×16)	7.5287	10.5035	14.2365	15.6587	16.0542
10	HSBQLP20 (20 × 20)	7.5263	10.4833	14.2170	15.5679	16.0437
	SBQLP (20 × 20) [34]	7. 4168	10. 4271	13. 9509	15. 5788	15. 8220
	p-Ritz (Liew) [77]	7. 411	10. 393	13. 913	15. 429	15. 806
	MISQ20 [47]	7. 4542	10. 5909	14. 0808	16. 0497	16. 0868
	HSBQLP20 (8×8)	11.1046	14.2101	21.8525	24.0092	24.9891
	HSBQLP20 (12 × 12)	11.0805	14.1334	20.9476	23.7557	25.1462
	HSBQLP20 (16×16)	11.0728	14.1191	20.6972	23.6664	25.2138
	HSBQLP20 (20 × 20)	11.0694	14.1144	20.5917	23.6249	25.2466
	SBQLP (20 × 20) [34]	10. 9664	14. 0480	20. 5667	23. 2866	24. 9647
	p-Ritz (Liew) [77]	10. 953	14. 028	20. 388	23. 196	24. 978
20	MISQ20 [47]	11. 0454	14. 2988	21. 4609	23. 6389	25. 4605
	HSBQLP20 (8×8)	14.6200	17.4030	25.9367	39.3689	39.6588
	HSBQLP20 (12 × 12)	14.5122	17.3362	24.7094	37.3000	38.6220
	HSBQLP20 (16×16)	14.4811	17.3542	24.4748	36.2394	38.2727
	HSBQLP20 (20 × 20)	14.4675	17.3678	24.3908	35.8243	38.1146
	SBQLP (20 × 20) [34]	14. 7043	17. 6157	24. 6527	36. 1657	39. 5037
	p-Ritz (Liew) [77]	14. 666	17. 614	24. 511	35. 532	39. 157
	MISQ20 [47]	14. 6199	17. 7013	25. 5625	38. 2411	39. 3269

4.2.1.2 Effect of aspect ratio on the non-dimensional response frequencies

In this example, the fundamental frequencies ($\bar{\beta}$) of a SSSS square cross plate ($[0^\circ/90^\circ/90^\circ/0^\circ]$) are listed in [Table 7](#). The analysis uses a mesh of 20x20, with the side-to-thickness ratio varying from 5 to 100. The purpose of this example is to examine the influence of the aspect ratio on the vibrational behavior of square laminated plates. The numerical results obtained from the current element are compared to several existing theories, including the higher-order transverse strain theory of Reddy and Phan[78], the p-Ritz solution of Liew[77], and a global higher-order plate theory presented by Matsunaga[79]. It is observed that the current results closely align with those from the referenced studies. However, they are more consistent with the p-Ritz solution of Liew[77].

Table 7. Influence of the aspect ratio on the non-dimensional frequency ($\bar{\beta}$) of a SSSS cross square plate [0°/90°/90°/0°].

Method	a/h					
	5	10	20	25	50	100
Present (20X20)	10.8500	15.1242	17.6315	18.0410	18.6419	18.8033
p-Ritz [77]	10.8550	15.1434	17.6583	18.0718	18.6734	18.8359
Reddy and Phan [78]	10.9891	15.2689	17.6669	18.0490	18.4624	18.7561
Matsunaga [79]	10.6876	15.0721	17.6369	18.0557	18.6702	18.8352

For a better illustration, Fig. 13 depicts the shows the impact of the aspect ratio a/h on the nondimensional natural frequencies of laminated square plate. The figure shows that as the aspect ratio increases, the undimensional frequencies increase.

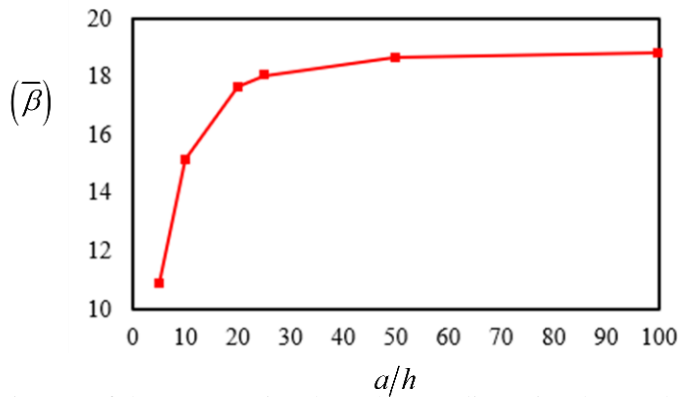


Figure 13. The impact of the aspect ratio a/h on the non-dimensional natural frequencies ($\bar{\beta}$) of SSSS cross square plate [0°/90°/90°/0°].

4.2.1.3 Effect of the number of layers and the degree of orthotropy on the natural frequencies

In the third example, a simply supported symmetric 3-layer [0°/90°/0°], 5-layer [0°/90°/0°/90°/0°], and 9-layer [0°/90°/0°/90°/0°/90°/0°/90°/0°] cross-ply laminated square plate are analyzed using materials M2, M3, M4, and M5, with their properties defined in Table 2. The dimensionless fundamental frequencies ($\bar{\Omega}$) for various orthotropy ratios are summarized in Table 8 for a side-to-thickness ratio of $a/h = 5$, using a mesh of 12x12. These results validated against with the numerical solutions obtained using the strain-based approach (SBQLP) of Belounar et al [34] based on FSDT, the layerwise approach (FEM-Q4-LW, FEM-Q9-LW)[80], and of the highest order [81]. For all three types of laminates plate, good agreement is observed with the mentioned references.

Fig. 14. Shows the variation in the dimensionless fundamental frequencies for three, five, and nine orthotropic layers (with a side-to-thickness ratio of $a/h=5$) as a function of the degree of orthotropy, represented by the (E_1/E_2) ratios. It can be observed that the dimensionless fundamental frequencies increase as the modulus ratio (E_1/E_2) increases. This is because an increase in the modulus ratio enhances the overall stiffness of the laminated plate, making the structure less flexible and more resistant to deformation, which results in higher fundamental frequencies. It can also be observed from the nine-layer laminate, with the highest number of layers and alternating fiber orientations, exhibits the greatest stiffness. As a result, it achieves the highest fundamental frequencies compared to the five-layer and three-layer laminates.

Table 8. Dimensionless natural frequency ($\bar{\Omega}$) of the SSSS square composite with different orthotropic layers and modulus ratios E_1/E_2 .

Model	Number of layers	E_1/E_2			
		3	10	20	30
Present (12 x 12)		0.2621	0.3282	0.3731	0.3982
SBQLP [34]		0.2619	0.3262	0.3694	0.3935
FEM-Q9-LW [80]	[0°/90°/0°]	0.2621	0.3262	0.3691	0.3927
FEM-Q 4 -LW [80]		0.2683	0.3297	0.3685	0.3886
FEM-Q9-HSDT [81]		0.2624	0.3264	0.3698	0.3941
FEM-Q4-HSDT [81]		0.2628	0.3270	0.3703	0.3947
Present (12 x 12)		0.2628	0.3368	0.3991	0.4354
SBQLP [34]		0.2627	0.3357	0.3917	0.4256
FEM-Q9-LW [80]	[0°/90°/0°/90°/0°]	0.2618	0.3330	0.3858	0.4166
FEM-Q 4 -LW [80]		0.2683	0.3396	0.3918	0.4219
FEM-Q9-HSDT [81]		0.2637	0.3373	0.3929	0.4258
FEM-Q4-HSDT [81]		0.2641	0.3378	0.3935	0.4264
Present (12 x 12)		0.2630	0.3399	0.4007	0.4377
SBQLP [34]		0.2631	0.3398	0.4002	0.4367
FEM-Q9-HSDT [81]	[0°/90°/0°/90°/0°/90°/0°/90°/0°]	0.2637	0.3373	0.3929	0.4258
FEM-Q4-HSDT [81]		0.2641	0.3378	0.3935	0.4264

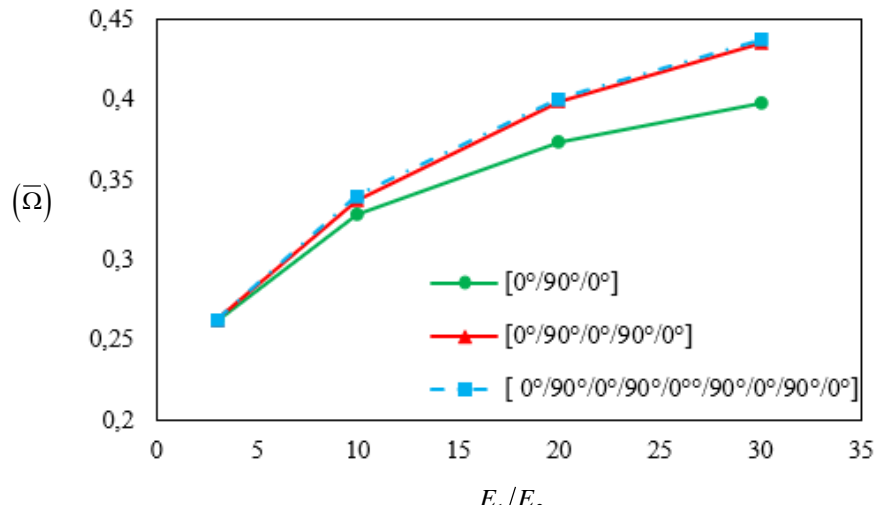


Figure 14 The effect of number of layers and the degree of orthotropy (E_1/E_2) on the dimensionless fundamental frequencies ($a/h=5$).

4.2.2 Skew laminated plates.

This research focuses on the normalized frequencies ($\bar{\omega}$) of five-layer skew laminated square plates with two stacking sequences : [45°/-45°/45°/-45°/45°] and [90°/0°/90°/0°/90°]. The plates are analyzed under (SSSS) and (CCCC) boundaries, with $a/h= 10$ and the material specified as M6 (see Table 2). A 13x13 node grid is used to model the plates, as shown in Figure 15. The study presents the normalized frequencies for the HSBQLP20 element, considering inclination angles (θ) from 0° to 60°, as depicted in Tables 9 and 10 for the two different stacking configurations. These findings are being compared with the results obtained by the MISQ20 approach [47], the MLSDQ presented by Liew et al. [77], the radially based method of Ferreira et al. [82], and the B-splines presented by Wang [83]. The proposed approach shows a high agreement with the previous findings for cross-ply and angle-ply composite plates. In addition, Figure 16 shows the first four mode shapes of the five-layer skew-flattened plate with the [90°/0°/90°/0°/90°] configuration.

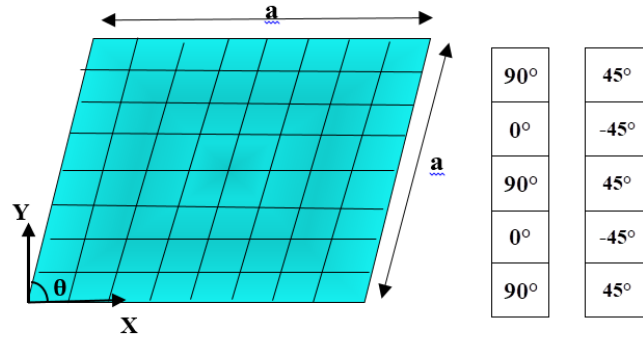


Figure 15. Geometry of inclined composite plate.

Table 9. Non-dimensional natural frequencies ($\bar{\omega}$) for a simply supported and clamped cross-laminated plate [90°/0°/90°/0°/90°] with different angles

Boundary	Theory	θ				
		0°	15°	30°	45°	60°
SSSS	Present (12x12)	1.5543	1.6690	2.0568	2.8647	4.5537
	MISQ20[47]	1.5733	1.6896	2.0820	2.8855	4.5412
	MLSDQ[77]	1.5709	1.6886	2.1026	2.8798	4.4998
	RBF[82]	1.5791	1.6917	2.0799	2.8228	4.3761
	FSDT[83]	1.5595	1.6697	2.0449	2.8126	4.3936
	HSDT[83]	1.5655	1.6787	2.0645	2.8598	4.5191
CCCC	Present (12x12)	2.3694	2.4611	2.77674	3.5005	5.0794
	MISQ20[47]	2.3869	2.4803	2.7998	3.4893	4.9989
	MLSDQ[77]	2.379	2.4725	2.7927	3.4723	4.943
	RBF[82]	2.4021	2.4932	2.8005	3.4923	4.9541
	FSDT[83]	2.3403	2.4327	2.7474	3.4245	4.8966
	HSDT[83]	2.3522	2.4497	2.7830	3.5038	5.0849

Table 10. Dimensionless fundamental frequencies ($\bar{\omega}$) for a SSSS and CCCC angle-ply-laminated plate [45°/-45°/45°/-45°/45°] with different angles

Boundary	Theory	θ				
		0°	15°	30°	45°	60°
SSSS	Present (12x12)	1.8785	1.93699	2.1194	2.6096	4.0856
	MISQ20[47]	1.8413	1.8889	2.0955	2.5672	3.971
	MLSDQ[77]	1.8248	1.8838	2.0074	2.5028	4.0227
	RBF[82]	1.8357	1.8586	2.0382	2.4862	3.8619
	FSDT[83]	1.8611	1.9097	2.1179	2.6068	4.0599
	HSDT[83]	1.8028	1.8279	2.0199	2.5105	3.9104
CCCC	Present (12x12)	2.2844	2.3627	2.6932	3.4453	4.9026
	MISQ20[47]	2.2908	2.3570	2.6708	3.3683	4.8982
	MLSDQ[77]	2.2787	2.3504	2.6636	3.3594	4.8566
	RBF[82]	2.3324	2.3962	2.6981	3.3747	4.8548
	FSDT[83]	2.2462	2.3109	2.6185	3.3009	4.7841
	HSDT[83]	2.2413	2.2763	2.5504	3.1921	4.6325

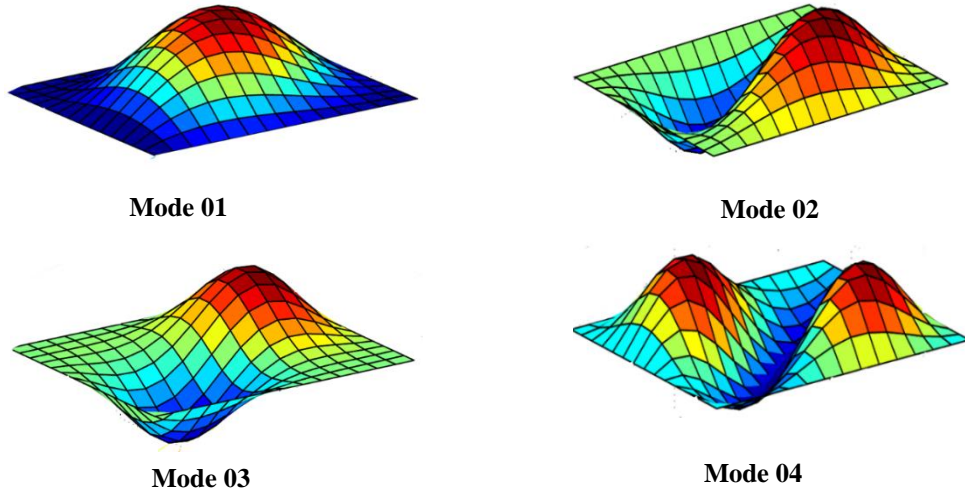


Figure 16. First 4 mode shapes of the five-layer skew CCCC plate [90°/0°/90°/0°/90°] with ($\theta = 30^\circ$, $a/h=10$).

4.2.3 Elliptical plates

Next, we investigate the dimensionless frequency ($\bar{\omega}$) of a 3-layer [0°/90°/0°] CCCC elliptically shaped plate, as depicted in Fig. 17a. The elliptical plate features two principal radii: $a = 5$ and $b = 2.5$, respectively. Material 7 is employed for this analysis. A mesh consisting of 680 elements is utilized to compute the non-dimensional frequencies, as illustrated in Fig. 17b. In the absence of an analytical result, the findings are compared with those obtained from the isogeometrical results based on the LW-FSDT [39], and isogeometric generalized analysis using TSDT, SSDT, and ESDT [40] for laminated composites. Table 11 provides a comparison of the first six dimensionless frequency between the current solution and other methods, with a length-to-thickness ratio of $a/h=10$. From Table 11, it can be observed that the present HSBQLP20 element shows excellent agreement with other solutions based on LW-FSDT [39], IGA-TSDT [40], IGA-SSDT [40], and IGA-ESDT [40]. In addition, Fig. 18 shows the first six mode shapes of a fully clamped three-layer [0°/90°/0°] composite ellipsoidal plate.

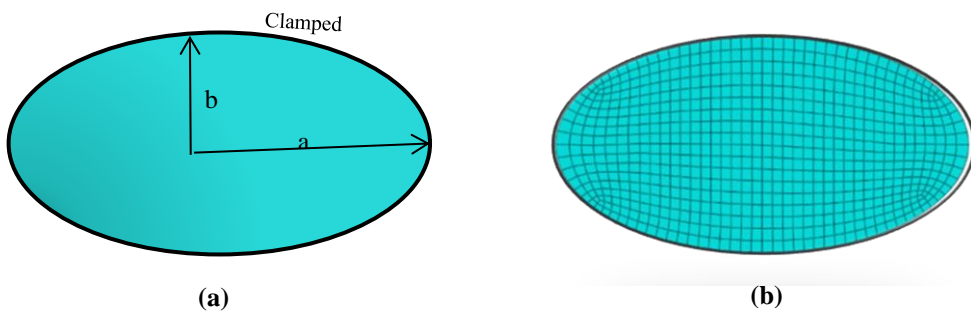


Figure 17. The geometries and a mesh-grid of a clamped elliptical plate.

Table 11. Normalized natural frequencies ($\bar{\omega}$) of a clamped three-layer [0°/90°/0°] of a ellipse plate.

Method	Modes					
	1	2	3	4	5	6
Present	17.1890	25.7460	37.0940	39.2080	49.1840	50.4010
IGA-LW-FSDT [39]	17.184	25.714	36.982	39.196	49.148	50.259
IGA-TSDT [40]	17.188	25.7979	37.0987	39.0942	49.1092	50.3576
IGA-SSDT [40]	17.2128	25.8318	37.1416	39.2032	49.2466	50.4108
IGA-ESDT [40]	17.2446	25.876	37.1991	39.3431	49.4234	50.484

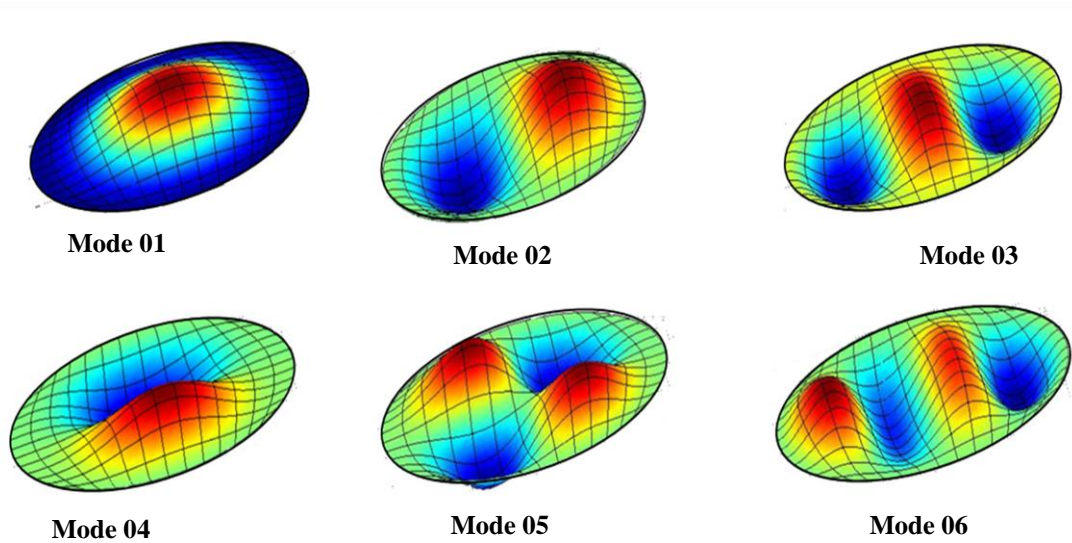


Figure 18. Six mode forms of a four-layer [0°/90°/0°] CCCC laminated elliptical plate (a/h=10).

4.2.4. Circular plates

In this example, a clamped circular four-layer laminated plate with the stacking sequence [θ/-θ/-θ/θ] and a diameter-to-thickness ratio of D/h = 10 is analyzed for different fiber orientation angles ($\theta = 15^\circ, 30^\circ, 45^\circ$). The plate is discretized using the mesh shown in [Fig. 19](#). The first six non-dimensional natural frequencies ($\bar{\beta} = (wD^2/h)(\rho/E_2)^{1/2}$), obtained using the present element with ($E_1/E_2 = 40$), are presented in [Table 12](#) and compared with results from other established elements.

The outcomes demonstrate that the proposed HSBQLP20 element provides results in excellent agreement with those obtained by bellounar SBQLP [34], MLSDQ [77], and MISQ20 [84] formulations. The first three corresponding mode shapes of the clamped circular four-layer [45°/-45°/45°/-45°] laminated plate are depicted in [Fig. 20](#).

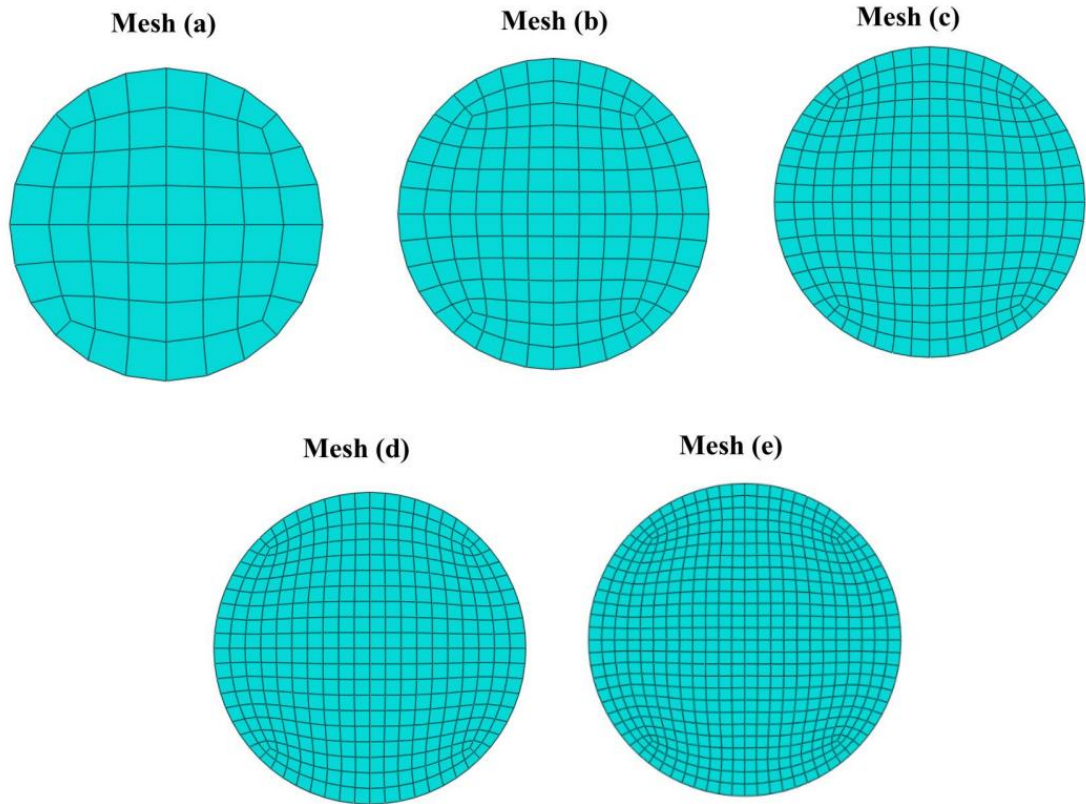


Figure 19. Circular plate models with different mesh densities: (a) 60, (b) 152, (c) 272, (d) 384, and (e) 588 quadrilateral elements

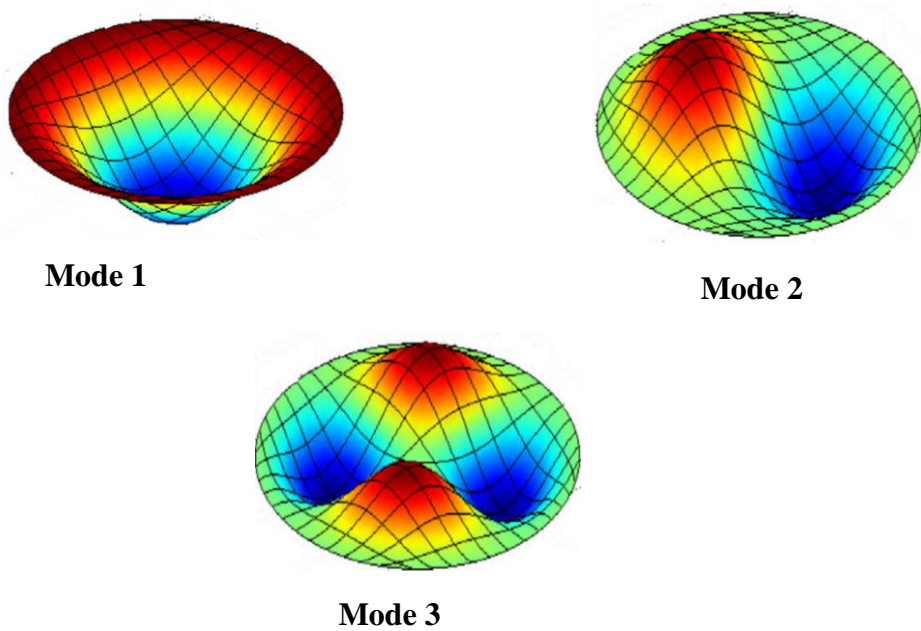


Figure 20. First three mode shapes of a clamped circular laminated plate with [45/-45/-45/45].

Table 12. Non-dimensional frequency ($\bar{\beta}$) for a clamped circular 4-layer laminated plate.

θ	Method	Modes					
		1	2	3	4	5	6
15°	HSBQLP20 (Mesh a)	22.4112	31.5132	42.9615	43.3117	52.5718	57.8220
	HSBQLP20 (Mesh b)	22.5613	31.2217	43.2518	43.5819	52.8820	58.2622
	HSBQLP20 (Mesh c)	22.6355	31.3325	43.3969	43.7012	53.0048	58.6259
	HSBQLP20 (Mesh d)	22.6512	31.3622	43.4215	43.7789	53.0569	58.8128
	HSBQLP20 (Mesh e)	22.6600	31.3738	43.4311	43.7857	53.0620	58.8525
	Bellounar SBQLP [34]	22.6565	31.3732	43.4306	43.7842	53.0588	58.8459
	MLSDQ [77]	22.774	31.455	43.350	43.469	52.872	57.386
	MISQ20 [84]	22.698	31.568	43.635	44.318	53.468	60.012
30°	HSBQLP20 (Mesh a)	23.6112	35.7813	43.4817	51.0220	56.3522	65.7825
	HSBQLP20 (Mesh b)	23.8320	36.0025	43.7033	51.2935	56.6905	66.1212
	HSBQLP20 (Mesh c)	23.9305	36.1012	43.8325	51.4236	56.8644	66.3850
	HSBQLP20 (Mesh d)	23.9569	36.1214	43.9425	51.4602	56.9608	66.5625
	HSBQLP20 (Mesh e)	23.9630	36.1305	43.9502	51.4705	56.9755	66.6008
	Bellounar SBQLP [34]	23.9625	36.1299	43.9477	51.4653	56.9742	66.5968
	MLSDQ [77]	24.071	36.153	43.968	51.074	56.315	66.220
	MISQ20 [84]	24.046	36.399	44.189	52.028	57.478	67.099
45°	HSBQLP20 (Mesh a)	24.3112	38.6825	43.1233	56.7240	56.8150	65.0960
	HSBQLP20 (Mesh b)	24.5225	38.8935	43.3840	56.9825	57.0280	65.4295
	HSBQLP20 (Mesh c)	24.6312	39.0225	43.5235	57.1540	57.2242	65.6750
	HSBQLP20 (Mesh d)	24.6566	39.0705	43.5625	57.2322	57.3425	65.7923
	HSBQLP20 (Mesh e)	24.6688	39.0901	43.5827	57.2526	57.3660	65.8102
	Bellounar SBQLP [34]	24.6585	39.0893	43.5772	57.2413	57.3567	65.8039
	MLSDQ [77]	24.752	39.181	43.607	56.759	56.967	65.571
	MISQ20 [84]	24.766 3	39.441	43.817	57.907	57.945	66.297

4.2.5. Triangular laminated plates

In this example, fully clamped triangular laminated plates with a side-to-thickness ratio of $a/h=100$ are analyzed for both angle-ply [$45^\circ/-45^\circ$] and cross-ply [$0^\circ/90^\circ/0^\circ$] configurations. The plate is discretized using a mesh of 384 quadrilateral elements, as illustrated in Figure. 21, and the material properties correspond to material type M1 (see Table 2).

The first six non-dimensional frequencies ($\bar{\beta}$) obtained using the present element are summarized in Table 13, while the corresponding mode shapes are illustrated in Figure. 22.

The present results show excellent agreement with those reported for the MISQ20 element [84] and the element developed by Bellounar et al. [34], confirming the accuracy and reliability of the proposed formulation for triangular laminated plates.

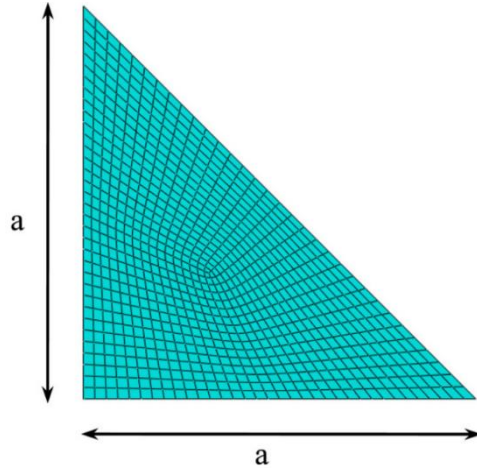


Figure 21. Meshing of the triangular plate with 832 quadrilateral elements..

Table 13. Non-dimensional frequency ($\bar{\beta}$) of a clamped laminated triangular plate.

Lay-up	Method	Modes					
		1	2	3	4	5	6
[45°/-45°]	HSBQLP20	52.635	86.669	112.683	130.856	156.915	185.645
	Bellounar [34]	52.585	86.586	112.573	130.654	156.824	185.623
	MISQ20 [84]	52.571	86.269	113.882	130.911	160.286	186.491
[0°/90°/0°]	HSBQLP20	69.996	108.895	146.570	159.977	199.812	217.363
	Bellounar [34]	69.939	108.728	146.459	159.309	199.549	217.025
	MISQ20 [84]	70.000	109.088	148.223	160.771	203.320	221.969

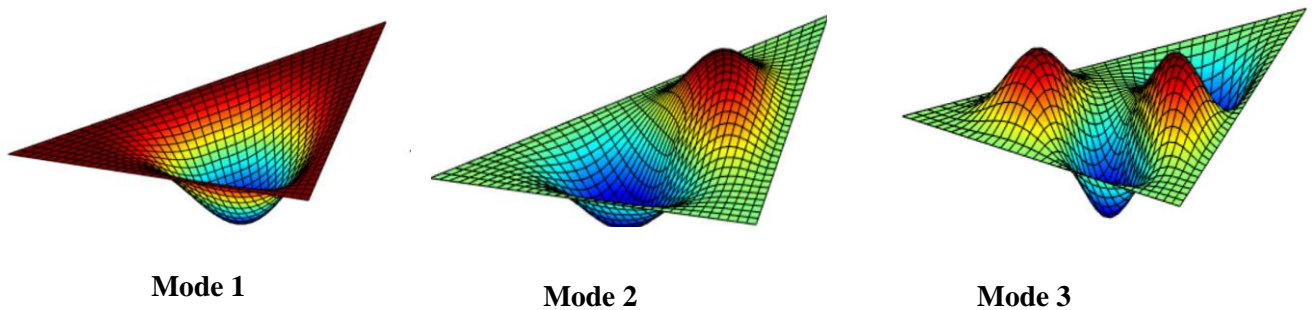


Figure22. First three mode shapes of a fully clamped [45°/-45°] laminated triangular plate.

4. Conclusion

The static and free vibration behaviors of laminated composite square, skew, elliptical and circular plates have been investigated using the HSBQLP20 finite element model, which is based on the strain approach and the new trigonometric shear deformation theory (TSDT). This model assumes a sinusoidal lateral shear stress distribution through the plate's thickness, with zero values at the free surfaces. The displacement functions for the HSBQLP20 element are formulated within the strain-based approach, utilizing assumed strain functions that ensure compatibility with the governing equations.

To validate its effectiveness, the element was applied to various symmetric and antisymmetric laminated composite plates with varying geometries, boundary conditions, layering sequences, and loading types. Comparisons with both analytical and numerical solutions from previous studies highlighted its superior precision and performance in the computation of bending and free vibrational behavior.

In perspective, the finite element model presented here provides a robust numerical model for the simulation and evaluation of layered composite plates. It will be extended in the future for the study of composites plates and also for the study of composite shell geometries..

Disclosure statement: I have no conflicts of interest to declare.

References

- [1] Nguyen N, Nguyen H, Phan D-H, Nguyen-Xuan H (2017) A polygonal finite element method for laminated composite plates. *Int J Mech Sci* 133:863-882.
- [2] Noor AK (1973) Free vibrations of multilayered composite plates. *AIAA J* 11(7):1038-1039.
- [3] Pagano NJ (1970) Exact solutions for rectangular bidirectional composites and sandwich plates. *J Compos Mater* 4(1):20-34.
- [4] Reddy JN (2003) Mechanics of laminated composite plates and shells: theory and analysis. CRC Press.
- [5] Ferreira AJM (2005) Analysis of composite plates using a layerwise theory and multiquadratics discretization. *Mech Adv Mater Struct* 12(2):99-112.
- [6] Liu B, Ferreira AJM, Xing YF, Neves AMA (2016) Analysis of composite plates using a layerwise theory and a differential quadrature finite element method. *Compos Struct* 156:393-398.
<https://doi.org/10.1016/j.compstruct.2015.07.101>
- [7] Alam MI, Pandit MK, Pradhan AK (2024) A modified higher-order zigzag theory for predicting flexural behavior of laminated composite and sandwich shell. *Mech Adv Mater Struct* 31(25):6434-6449.
- [8] Sahoo R, Singh BN (2015) Assessment of inverse trigonometric zigzag theory for stability analysis of laminated composite and sandwich plates. *Int J Mech Sci* 101-102:145-154.
<https://doi.org/10.1016/j.ijmecsci.2015.07.023>
- [9] Shao D, Wang Q, Tao Y, Shao W, Wu W (2021) A unified thermal vibration and transient analysis for quasi-3D shear deformation composite laminated beams with general boundary conditions. *Int J Mech Sci* 198:106357. <https://doi.org/10.1016/j.ijmecsci.2021.106357>
- [10] Mantari JL, Soares CG (2014) Four-unknown quasi-3D shear deformation theory for advanced composite plates. *Compos Struct* 109:231-239.

- [11] Wang X, Shi G (2015) A refined laminated plate theory accounting for the third-order shear deformation and interlaminar transverse stress continuity. *Appl Math Model* 39(18):5659-5680. <https://doi.org/10.1016/j.apm.2015.01.030>
- [12] Reddy JN (1984) A simple higher-order theory for laminated composite plates.
- [13] Gao YS, Cai CS, Huang CY, Zhu QH, Schmidt R, Zhang SQ (2024) A compressible layerwise third-order shear deformation theory with transverse shear stress continuity for laminated sandwich plates. *Compos Struct* 338:118108. <https://doi.org/10.1016/j.compstruct.2024.118108>
- [14] Aagaah MR, Mahinfalah M, Jazar GN (2006) Natural frequencies of laminated composite plates using third order shear deformation theory. *Compos Struct* 72(3):273-279. <https://doi.org/10.1016/j.compstruct.2004.11.012>
- [15] Jun L, Li J, Xiaobin L (2017) A spectral element model for thermal effect on vibration and buckling of laminated beams based on trigonometric shear deformation theory. *Int J Mech Sci* 133:100-111. <https://doi.org/10.1016/j.ijmecsci.2017.07.059>
- [16] Mantari JL, Oktem AS, Guedes Soares C (2012) A new trigonometric shear deformation theory for isotropic, laminated composite and sandwich plates. *Int J Solids Struct* 49(1):43-53. <https://doi.org/10.1016/j.ijsolstr.2011.09.008>
- [17] Thai CH, Ferreira AJM, Bordas SPPA, Rabczuk T, Nguyen-Xuan H (2014) Isogeometric analysis of laminated composite and sandwich plates using a new inverse trigonometric shear deformation theory. *Eur J Mech A Solids* 43:89-108.
- [18] Mantari JL, Oktem AS, Guedes Soares C (2012) A new trigonometric layerwise shear deformation theory for the finite element analysis of laminated composite and sandwich plates. *Comput Struct* 94-95:45-53. <https://doi.org/10.1016/j.compstruc.2011.12.003>
- [19] Mantari JL, Oktem AS, Guedes Soares C (2011) Static and dynamic analysis of laminated composite and sandwich plates and shells by using a new higher-order shear deformation theory. *Compos Struct* 94(1):37-49. <https://doi.org/10.1016/j.compstruct.2011.07.020>
- [20] Sayyad AS (2013) Flexure of thick orthotropic plates by exponential shear deformation theory. *Lat Am J Solids Struct* 10:473-490.
- [21] Bendahane K, Sehouli M, Bouguenina O, Benahmed A (2024) Vibration analysis using the theory of exponential shear deformation for laminated plates. *J Eng Exact Sci* 10(7):19977-19977.
- [22] El Meiche N, Tounsi A, Ziane N, Mechab I, Bedia EAA (2011) A new hyperbolic shear deformation theory for buckling and vibration of functionally graded sandwich plate. *Int J Mech Sci* 53(4):237-247.
- [23] Grover N, Maiti DK, Singh BN (2013) A new inverse hyperbolic shear deformation theory for static and buckling analysis of laminated composite and sandwich plates. *Compos Struct* 95:667-675. <https://doi.org/10.1016/j.compstruct.2012.08.012>
- [24] Shishehsaz M, Raissi H, Moradi S (2020) Stress distribution in a five-layer circular sandwich composite plate based on the third and hyperbolic shear deformation theories. *Mech Adv Mater Struct* 27(11):927-940.
- [25] Akavci SS, Tanrikulu AH (2008) Buckling and free vibration analyses of laminated composite plates by using two new hyperbolic shear-deformation theories. *Mech Compos Mater* 44:145-154.

- [26] Thai H-T, Kim S-E (2010) Free vibration of laminated composite plates using two variable refined plate theory. *Int J Mech Sci* 52(4):626-633. <https://doi.org/10.1016/j.ijmecsci.2010.01.002>
- [27] Tran LV, Thai CH, Le HT, Gan BS, Lee J, Nguyen-Xuan H (2014) Isogeometric analysis of laminated composite plates based on a four-variable refined plate theory. *Eng Anal Bound Elem* 47:68-81. <https://doi.org/10.1016/j.enganabound.2014.05.013>
- [28] Suleyman Adak (2024) Power Factor Analysis of Grid-Connected Solar Inverter under Different Irradiance Levels throughout the Day. *Energies* 17(15), 3632; <https://doi.org/10.3390/en17153632>
- [29] Zhou Y, Yao F, Wang Y, Bai C, Liu S (2025) Free vibration of orthotropic rectangular Mindlin plates via spectral element model under arbitrary boundary conditions. *Thin-Walled Structures* 216(C):113679. <https://doi.org/10.1016/j.tws.2025.113679>
- [30] Tran KQ, Duong TV, Hoang T-D, Wahab MA, Hackl K, Nguyen-Xuan H (2025) A new thermoelastic model for agglomerated and randomly-oriented CNT-reinforced bio-inspired materials: Temperature-dependent free vibration analysis of FG-CNTR-TPMS plates. *Engineering Analysis with Boundary Elements* 174:106157. <https://doi.org/10.1016/j.enganabound.2025.106157>
- [31] Zhou Y, Yao F, Bai C, Li K, Zhu S, Wahab MA (2024) Bandgap characteristics of periodic Mindlin plates under arbitrary boundary conditions via the Spectral Element Method. *Thin-Walled Structures* 205(B):112370. <https://doi.org/10.1016/j.tws.2024.112370>
- [32] Qin S, Feng J, Tang J, Huo X, Zhou Y, Yang F, Wahab MA (2024) Condition assessment of a concrete filled steel tube arch bridge using in-situ vibration measurements and an Improved Artificial Fish Swarm Algorithm. *Computers & Structures* 291:107213. <https://doi.org/10.1016/j.compstruc.2023.107213>
- [33] Qin S, Tang J, Wahab MA (2023) Modal parameter identification in civil structures via Hilbert transform ensemble with improved empirical wavelet transform. *Journal of Vibration and Control* 30(7-8). <https://doi.org/10.1177/10775463231166428>
- [34] Belounar A, Belounar L, Tati A (2023) An assumed strain finite element for composite plates analysis. *Int J Comput Methods* 20(1):2250034. <https://doi.org/10.1142/S0219876222500347>
- [35] Zou Z (1998) Free vibration analysis of composite laminated right triangular plates with the finite-element method. *Mech Compos Mater Struct* 5(1):25-39.
- [36] Jun L, Hongxing H, Rongying S (2008) Dynamic finite element method for generally laminated composite beams. *Int J Mech Sci* 50(3):466-480. <https://doi.org/10.1016/j.ijmecsci.2007.09.014>
- [37] Shi P, Dong C, Sun F, Liu W, Hu Q (2018) A new higher order shear deformation theory for static, vibration and buckling responses of laminated plates with the isogeometric analysis. *Compos Struct* 204:342-358.
- [38] Gupta A, Ghosh A (2019) Static and transient analysis of sandwich composite plates using isogeometric analysis. *Mech Adv Mater Struct* 26(1):81-87.
- [39] Thai CH, Ferreira AJM, Carrera E, Nguyen-Xuan H (2013) Isogeometric analysis of laminated composite and sandwich plates using a layerwise deformation theory. *Compos Struct* 104:196-214.
- [40] Thai CH, Ferreira AJM, Abdel Wahab M, Nguyen-Xuan H (2016) A generalized layerwise higher-order shear deformation theory for laminated composite and sandwich plates based on isogeometric analysis. *Acta Mech* 227(5):1225-1250.

- [41] Bui TQ, Nguyen MN, Zhang C (2011) An efficient meshfree method for vibration analysis of laminated composite plates. *Comput Mech* 48:175-193.
- [42] Dai KY, Liu GR, Lim KM, Chen XL (2004) A mesh-free method for static and free vibration analysis of shear deformable laminated composite plates. *J Sound Vib* 269(3):633-652. [https://doi.org/10.1016/S0022-460X\(03\)00089-0](https://doi.org/10.1016/S0022-460X(03)00089-0)
- [43] Kwak S, Kim K, Li Y, Pang C (2022) A meshfree method for free vibration analysis of ply drop-off laminated rectangular plates. *Mech Adv Mater Struct* 29(26):5443-5459.
- [44] Pan E, Yang B, Cai G, Yuan FG (2001) Stress analyses around holes in composite laminates using boundary element method. *Eng Anal Bound Elem* 25(1):31-40. [https://doi.org/10.1016/S0955-7997\(00\)00066-7](https://doi.org/10.1016/S0955-7997(00)00066-7)
- [45] Hsu C-W, Mittelstedt C, Hwu C (2024) Boundary element method for bending-extension coupling shear deformable laminated composite plates with multiple stiffeners. *Eng Anal Bound Elem* 164:105757. <https://doi.org/10.1016/j.enganabound.2024.105757>
- [46] Sollero P, Aliabadi MH (1995) Anisotropic analysis of cracks in composite laminates using the dual boundary element method. *Compos Struct* 31(3):229-233. [https://doi.org/10.1016/0263-8223\(95\)00105-0](https://doi.org/10.1016/0263-8223(95)00105-0)
- [47] Nguyen-Van H, Mai-Duy N, Tran-Cong T (2008) Free vibration analysis of laminated plate/shell structures based on FSDT with a stabilized nodal-integrated quadrilateral element. *J Sound Vib* 313(1-2):205-223.
- [48] Nguyen-Van H, Mai-Duy N, Karunasena W, Tran-Cong T (2011) Buckling and vibration analysis of laminated composite plate/shell structures via a smoothed quadrilateral flat shell element with in-plane rotations. *Comput Struct* 89(7-8):612-625.
- [49] Thai-Hoang C, Nguyen-Thanh N, Nguyen-Xuan H, Rabczuk T (2011) An alternative alpha finite element method with discrete shear gap technique for analysis of laminated composite plates. *Appl Math Comput* 217(17):7324-7348.
- [50] Phan-Dao HH, Nguyen-Xuan H, Thai-Hoang C, Nguyen-Thoi T, Rabczuk T (2013) An edge-based smoothed finite element method for analysis of laminated composite plates. *Int J Comput Methods* 10(1):1340005.
- [51] Katili I, Maknun IJ, Batoz JL, Katili AM (2018) Asymptotic equivalence of DKMT and MITC3 elements for thick composite plates. *Compos Struct* 206:363-379.
- [52] Belounar A, Benmebarek S, Belounar L (2020) Strain based triangular finite element for plate bending analysis. *Mech Adv Mater Struct* 27(8):620-632.
- [53] Ashwell DG, Sabir AB (1972) A new cylindrical shell finite element based on simple independent strain functions. *Int J Mech Sci* 14(3):171-183.
- [54] Ashwell DG, Sabir AB, Roberts TM (1971) Further studies in the application of curved finite elements to circular arches. *Int J Mech Sci* 13(6):507-517.
- [55] Sabir AB (1985) A rectangular and triangular plane elasticity element with drilling degrees of freedom. In: Proceedings of the Second International Conference on Variational Methods in Engineering. Brebbia CA (ed.), Southampton University, pp. 17-25.

- [57] Belarbi MT, Maalem T (2005) On improved rectangular finite element for plane linear elasticity analysis. *Rev Eur Elem* 14(8):985-997.
- [58] Rebiai C, Belounar L (2013) A new strain based rectangular finite element with drilling rotation for linear and nonlinear analysis. *Arch Civ Mech Eng* 13:72-81.
- [59] Belarbi MT, Charif A (1999) Développement d'un nouvel élément hexaédrique simple basé sur le modèle en déformation pour l'étude des plaques minces et épaisses. *Rev Eur Elem Finis* 8(2):135-157.
- [60] Belounar L, Guerraiche K (2014) A new strain based brick element for plate bending. *Alex Eng J* 53(1):95-105. <https://doi.org/10.1016/j.aej.2013.10.004>
- [61] Messai A, Belounar L, Merzouki T (2018) Static and free vibration of plates with a strain based brick element. *Eur J Comput Mech*:1-21.
- [62] Belounar A, Benmebarek S, Houhou MN, Belounar L (2019) Static, free vibration, and buckling analysis of plates using strain-based Reissner–Mindlin elements. *Int J Adv Struct Eng* 11 :211-230.
- [63] Belounar A, Benmebarek S, Houhou MN, Belounar L (2020) Free vibration with Mindlin plate finite element based on the strain approach. *J Inst Eng India C* 101:331-346.
- [64] Sadgui A, Tati A (2022) A Novel Trigonometric Shear Deformation Theory for the Buckling and Free Vibration Analysis of Functionally Graded Plates. *Mech Adv Mater Struct* 29 (27) : 6648–6663. <https://doi.org/10.1080/15376494.2021.1983679>.
- [65] Tati A (2021) A Five Unknowns High Order Shear Deformation Finite Element Model for Functionally Graded Plates Bending Behavior Analysis. *J Braz Soc Mech Sci Eng* 43 (1) : 1–14. <https://doi.org/10.1007/s40430-020-02736-1>.
- [66] Hosseini-Hashemi S, Fadaee M, Es'haghi M (2010) A novel approach for in-plane/out-of-plane frequency analysis of functionally graded circular/annular plates. *Int J Mech Sci* 52 :1025–1035. <https://doi.org/10.1016/j.ijmecsci.2010.05.005>.
- [67] Cukanovic D, Radakovic A, Bogdanovic G, Milanovic M, Redzovic H, Dragovic D (2018) New shape function for the bending analysis of functionally graded plates. *Materials* 11(12):2381. <https://doi.org/10.3390/ma1112238>
- [68] Soldatos KP (1992) A transverse shear deformation theory for homogeneous monoclinic plates. *Acta Mech.* 94:195–220. <https://doi.org/10.1007/BF01176602>
- [69] Mechab B, Mechab I, Benaissa S (2012) Analysis of thick orthotropic laminated composite plates based on higher order shear deformation theory by the new function under thermo-mechanical loading. *Compos. Part B Eng.* 43:1310–1319. <https://doi.org/10.1016/j.compositesb.2011.11.037>
- [70] Adim B, Daouadji TH, Rabahi A (2016) A simple higher order shear deformation theory for mechanical behavior of laminated composite plates. *Int J Adv Struct Eng* 8(2):103–117
- [71] Assas T, Bourezane M, Chenafi M (2024) Static, free vibration, and buckling analysis of functionally graded plates using the strain-based finite element formulation. *Arch Appl Mech* 94(8):2243-2267. <https://doi.org/10.1007/s00419-024-02635-0>
- [72] Belounar A, Boussem F, Tati A (2022) A Novel C0 Strain-Based Finite Element for Free Vibration and Buckling Analyses of Functionally Graded Plates. *J Vib Eng Technol* 11(1):281–300. <https://doi.org/10.1007/s42417-022-00577-x>.

- [73] Belounar A, Belounar L (2025) An improved first-order strain-based finite element model with in-plane drilling rotation for static bending and free vibration analysis of functionally graded plates. *Mech Based Des Struct Mach.* <https://doi.org/10.1080/15397734.2025.2458089>
- [74] Pagang NJ, Hatfield SJ (1972) Elastic behavior of multilayered bidirectional composites. *AIAA J* 10(7):931–933.
- [75] Akhras G, Cheung MS, Li W (1994) Finite strip analysis of anisotropic laminated composite plates using higher-order shear deformation theory. *Comput Struct* 52(3):471–477.
- [76] Daghia F, de Miranda S, Ubertini F, Viola E (2008) A hybrid stress approach for laminated composite plates within the first-order shear deformation theory. *Int J Solids Struct* 45(6):1766–1787. <https://doi.org/10.1016/j.ijsolstr.2007.10.020>
- [77] Liew KM (1996) Solving the vibration of thick symmetric laminates by Reissner/Mindlin plate theory and the p-Ritz method. *J Sound Vib* 198(3):343–360.
- [78] Reddy JN, Phan N (1985) Stability and vibration of isotropic, orthotropic and laminated plates according to a higher-order shear deformation theory. *J Sound Vib* 98(2):157–170.
- [79] Matsunaga H (2000) Vibration and stability of cross-ply laminated composite plates according to a global higher-order plate theory. *Compos Struct* 48(4):231–244
- [80] Marjanović M, Vuksanović D (2014) Layerwise solution of free vibrations and buckling of laminated composite and sandwich plates with embedded delaminations. *Compos Struct* 108:9–20
- [81] Nayak AK, Moy SSJ, Shenoi RA (2002) Free vibration analysis of composite sandwich plates based on Reddy's higher-order theory. *Compos Part B Eng* 33(7):505–519.
- [82] Ferreira AJM, Roque CMC, Jorge RMN (2005) Free vibration analysis of symmetric laminated composite plates by FSDT and radial basis functions. *Comput Methods Appl Mech Eng* 194(39–41):4265–4278
- [83] Wang S (1997) Free vibration analysis of skew fibre-reinforced composite laminates based on first-order shear deformation plate theory. *Comput Struct* 63(3):525–538.
- [84] Nguyen-Van H, Mai-Duy N, Tran-Cong T (2008) Free vibration analysis of laminated plate/shell structures based on FSDT with a stabilized nodal-integrated quadrilateral element. *J. Sound Vib.* 313:205–223. <https://doi.org/10.1016/j.jsv.2007.12.003>